SEDIMENTATION OF PMMA SPHERES

By

STEVEN EDWARD PAULIN

Bachelor of Science

Cleveland State University

Cleveland, Ohio

1986

Submitted to the Faculty of the
Graduate College of the
Oklahoma State University
in partial fulfillment of
the requirements for
the Degree of
MASTER OF SCIENCE
July, 1990

SEDIMENTATION OF
PMMA SPHERES

Thesis Approved:

Thesis Adviser

Dean of the Graduate College

ACKNOWLEDGMENTS

I would like to thank my advisor, Dr. Bruce J. Ackerson for his careful guidance and inspiration throughout this project, as well as the other members of my committe: Dr. George S. Dixon and Dr. Hugh L. Scott. I would like to deeply thank my parents, Edward and Mary Jane, for their constant support throughout my education and my beautiful wife Carol, who has made this past year at Oklahoma State University more endurable. I would also like to express my gratitude to Mark Petrovic, Dr. W. Scott McCullough and Dr. Edward G. Behrens for their friendly advice and help with the LaTeX processing of this manuscript.

This acknowledgment would not be complete without the mention of Dr. P. D. Hambourger and Dr. T. W. Taylor who both gave me the opportunity, as an undergraduate, to work in their laboratories and Dr. Jack A. Soules who gave me the confidence not to give up. This work has been supported by the U. S. Department of Energy Grant DE/FG05/88ER45349.

TABLE OF CONTENTS

Chapter		Page
I.	INTRODUCTION	1
II.	THEORY	3
	Particle-Fluid Reference Frames	3
	Qualitative Fitting	4
	Pairwise Hydrodynamical Interactions	6
	Full N-body Hydrodynamical Interactions	7
III.	SAMPLES	8
	Materials	8
	Preparation	9
IV.	SETTLING EXPERIMENTS	12
	Sedimentation Height Measurements	12
	Phase Diagram	16
	Sedimentation Velocities	18
V.	EMPIRICAL AND THEORETICAL COMPARISON	23
VI.	SCATTERING MEASUREMENTS	26
VII.	CONCLUSIONS	33
BIBLIOGRAPHY		34
APPENDIXES		36
	APPENDIX A - A COPY OF PHYSICAL REVIEW LETTER IN WHICH SEDIMENTATION RESULTS ARE PUBLISHED	37
	APPENDIX B - HEIGHT VERSUS TIME DATA FOR ALL OTHER SAMPLES	42

Chapter Page

APPENDIX C - DENSITY PROFILES FOR ALL OTHER SAMPLES 55

LIST OF FIGURES

Figure — Page

1. Experimental set-up for sedimentation height measurements. 13

2. Sedimentaion height versus time for several samples of increasing volume fraction. Here (A) is clear supernatant, (B) colloidal liquid, (C) polycrystalline solid, (D) high density polycrystalline solid (E) columnar crystal sediment and (F) amorphous or glassy phases. 14

3. Phase diagram obtained from samples. Scaled and measured volume fractions are shown on the upper and lower horizontal axis, respectively. (L) is liquid, (C) coexistence, (X) crystal, and (G) glass phases, respectively. 17

4. The reduced sedimentation velocity from experimental data for liquid (○) and crystal (□) is shown. The theory of Beenakker and Mazur (●). 21

5. Close-up of the transition region with the theory of Zick and Homsy (■). (L) is liquid, (C) coexistence, (X) crystalline and (G) glass regions. 22

6. Comparison of reduced sedimentation velocity data with experimental data of other authors for ϕ_f^*. ($*$) this work, (○) Kops-Werkhoven and Fijnaut, and (□) Buscall et. al. 25

7. Experimental set-up for light scattering measurements showing image capture and storage capability. 27

8. Diagram depicting Bragg scattering from a crystallite in the cuvette to the imaging screen. Here n and n′ are the indices of refraction of the air and sample, respectively, a+d the distance of the crystallite from the screen and R the scattering ring radius. 29

Figure Page

9. Density profiles obtained from light scattering measurements over a period of $\sim$ three weeks. This figure corresponds to scattering from the columnar crystal region, (E) of a sample in the liquid region of the phase diagram. Here $\phi = 0.47$. 31

10. Density profiles obtained from light scattering measurements over a period of $\sim$ three weeks. This figure corresponds to scattering from the polycrystalline and dense polycrystalline regions, (C) and (D), respectively, of a sample in the coexistence region of the phase diagram. Here $\phi = 0.49$. 32

11. Sample in the liquid region of the phase diagram. $\phi = 0.099$. This is the lowest volume fraction sample observed. 43

12. Sample in the liquid region of the phase diagram. $\phi = 0.20$. 44

13. Sample in the liquid region of the phase diagram. $\phi = 0.29$. 45

14. Sample in the liquid region of the phase diagram. $\phi = 0.42$. 46

15. Sample in the liquid region of the phase diagram. $\phi = 0.42$. 47

16. Sample in the liquid region of the phase diagram. $\phi = 0.47$. 48

17. Sample in the liquid region of the phase diagram. $\phi = 0.47$. 49

18. Sample in the coexistence region of the phase diagram. $\phi = 0.48$. 50

19. Sample very near the freezing transition. The columnar crystal region (E) is qualified in quotes as this region did not appear to be true columnar crystal in observation, but some transitional phase to dense polycrystalline solid. $\phi = 0.49$. 51

20. Sample in the coexistence region of the phase diagram. $\phi = 0.50$. 52

21. Sample in the coexistence region of the phase diagram. $\phi = 0.51$. 53

22. Sample in the glass region of the phase diagram. Here the glass region (F) is qualified in quotes as this sample appeared transitional from fully crystalline to glass. $\phi = 0.57$. 54

23. Sample in the liquid region of the phase diagram. $\phi = 0.42$. 56

24. Sample in the liquid region of the phase diagram. $\phi = 0.46$. 57

25. Sample in the coexistence region of the phase diagram. $\phi = 0.48$. 58

Figure

Page

26. Sample in the coexistence region of the phase diagram. $\phi = 0.50$..... 59

27. Sample in the coexistence region of the phase diagram. $\phi = 0.51$..... 60

28. Sample in the fully crystalline region of the phase diagram. $\phi = 0.54$..... 61

29. Sample in the glass region of the phase diagram. This sample appeared transitional from fully crystalline to glass. $\phi = 0.57$..... 62

30. Sample in the glass region of the phase diagram. $\phi = 0.59$..... 63

CHAPTER I

INTRODUCTION

The hard sphere interaction of particles provides a simple but rich and important statistical mechanical model of condensed matter. The melting/freezing transition has been demonstrated via molecular dynamics[1] and studied most recently via density functional theory.[2] The liquid phase structure is modeled by the Wertheim-Thiel[3] solution to the Percus-Yevick equation and the Carnahan-Starling equation[4] correlates the thermodynamic results of computer simulations. In hard sphere perturbation theory, many of these results are used as the basis for calculating more accurate thermodynamic properties in a perturbation expansion about the hard sphere state.[5]-[7] In general, these approximations are necessary because no particles interact via a true hard sphere potential. However, recently the thermodynamic and statistical properties of ideal hard sphere systems have been used to interpret the results of experiments on colloidal suspensions of sterically stabilized particles.[8]-[13] These particles interact via a short ranged repulsive interaction with the stabilizing layer mitigating any van der Waals attractive forces. Compared to the charge stabilized interactions of colloidal particles or the typical interactions of atomic particles, these interactions may prove to be the best realization of the hard sphere interparticle potential.

The nonequilibrium properties of suspended particles differ from that for purely atomic systems due to the presence of a solvent which introduces hydrodynamical forces. Much theoretical work has been directed toward understanding nonequilibrium properties of model hard sphere suspensions,[14]-[20] again providing a basis for understanding more complex systems having other interparticle

interactions. Experimental data for nonequilibrium processes in suspensions of hard spheres is limited but serves as an important check of theoretical results.

In this study, the sedimentation of locally equilibrating hard spheres is observed, in which formation of liquid like or polycrystalline ordering occurs before there is significant sedimentation of the suspension. As a result, measurements of the sedimentation velocity have been made for randomly stacked polycrystalline phases at large volume fraction and for liquid-like phases at low volume fractions. The melting/freezing phase transition is observed in the reduced sedimentation velocity as a function of the particle volume fraction and serves as a definitive marker for comparison with theoretical results. These experimental results differ in one aspect or another from others reported for "hard" sphere suspensions [8]-[13,21,22] in that they extend to large volume fractions, the particles are not charged and a melting/freezing transition is observed. The failure to observe a melting/freezing transition in other work may have resulted from not having hard sphere interactions, a polydispersity of particle size, or a sedimentation rate greater than the nucleation and growth rate for crystallites. The last condition will result in an amorphous interparticle ordering during sedimentation despite the lower free energy of the equilibrium crystal phase. An order/disorder transition has been reported for the sedimentation of "hard" spheres,[9] but this is a sedimentation induced crystallization where the increase in particle concentration on sedimentation triggers crystallization.

CHAPTER II

THEORY

When one considers the number of variables associated with a fluid-particle system, formulation of a quantitative model which is generally applicable to a wide variety of problems is both complex and often times unattainable. Characterization of such a system must include the following elements:[23] 1) The temperature, pressure and viscosity dependence of the fluid. 2) The density, size, and shape of the particles. Also the polydispersity, volume fraction, Brownian motion and distribution of particles within the fluid medium. 3) Motion of the particle and fluid phases relative to the containing vessel boundaries and relative to one another, the interparticle potential and possibly the surface characteristics of the particle. Below, a brief description of three approaches for calculating the sedimentation velocity of an assemblage of particles as well as a discussion of reference frames for the velocity used in these calculations, will be presented.

Particle-Fluid Reference Frames

The sedimenation velocity of the spheres must be relative to some reference frame. One has the choice of either the volume fixed or the solvent fixed reference frame. Experimentally, if one has a vessel in which the sedimentation of spheres is being observed, the sample is in a volume fixed reference frame. That is, the particle-fluid system, as confined to the vessel, maintains a total fixed volume. Let v_ϕ be the sedimentation velocity of the spheres as measured in the laboratory. Here the total volume flux, J_V, is zero,

$$J_V = \phi v_\phi + (1 - \phi) v_{solv} = 0 \tag{1}$$

where ϕ is the particle volume fraction and v_{solv} the solvent velocity also relative to the laboratory. In the volume fixed frame, the downward volume particle flux is balanced by a back flow of solvent which has been displaced by the particles. In some theories a solvent fixed reference frame is used, where the backflow is set to zero. That is, the velocity of the sedimenting particles in the solvent fixed reference frame, v_{part}, is related to the velocity of the sedimenting particles in the volume fixed frame as,

$$v_{part} = v_\phi - v_{solv}.$$

Solving Eq. 1 for v_{solv} and substituting the result into the above gives,

$$v_{part} = \frac{v_\phi}{(1-\phi)} \tag{2}$$

resulting in a $(1-\phi)$ correction for comparison of solvent fixed frame theories with volume fixed frame experiments.

Qualitative Fitting

In 1958, Maude and Whitmore[19] argued in the following manner for a form of the concentration dependent sedimentation velocity applicable to a wide variety of colloidal dispersions. Let F be the average force on the particles in a system of given volume fraction ϕ. If a small number of particles are added to the system and the velocity of sedimentation, v_ϕ, is assumed to be held constant, the solvent is no longer able to flow through those regions which are now occupied by the newly added particles and thus the solvent velocity, v_{solv}, through the suspension must increase. This results in an increase in the average force on the particles already present. This change in average force with respect to concentration is

$$\left(\frac{\partial F}{\partial \phi}\right)_{v_\phi} d\phi. \tag{3}$$

The same increase in average force may be obtained had the sedimentation velocity, v_ϕ, been increased by an amount dv_ϕ while the concentration, ϕ, is held constant. i.e.

$$\left(\frac{\partial F}{\partial v_\phi}\right)_{\phi} dv_\phi. \tag{4}$$

They further argue that the change in sedimentation velocity in the laboratory reference frame, dv_ϕ, must be proportional to both a change in concentration, $d\phi$, and the particle velocity in the solvent fixed reference frame, v_{part}. Thus,

$$dv_\phi = \beta v_{part} d\phi \tag{5}$$

where β is a constant of proportionality. It is believed that β depends only upon the distribution of solvent around each isolated particle and thus not be concentration dependent.

Using Eqs. 2, 3, 4 and 5 one may write,

$$\left(\frac{\partial F}{\partial \phi}\right)_{v_\phi} = \left(\frac{\partial F}{\partial v_\phi}\right)_\phi \frac{\beta v_\phi}{(1-\phi)} \tag{6}$$

from which it is suggested,

$$v_\phi = v_o(1-\phi)^\beta. \tag{7}$$

Experimental data for volume fractions ranging from $0 < \phi < 0.50$ has been fit to Eq. 7 for systems ranging from red blood cells to glass spheres in water as well as a host of other materials listed in reference[19]. Here v_o is the sedimentation velocity of an isolated particle acted upon by gravity. β represents a shape factor which varies with particle shape, but is approximately determined to be 5 for dispersions of monodisperse spheres.

A similar equation,

$$v = v_{Stokes}(1-\phi/p)^{kp}$$

has been used by reference[21] for polystyrene latex dispersions of radius 1.55μm in salt solutions. Here,

$$v_{Stokes} = 2ga^2(\rho_p - \rho_s)/9\eta \tag{8}$$

is the sedimentation velocity of an isolated sphere acted upon by gravity, where g is the acceleration due to gravity, ρ_p and ρ_s the density of the sphere and solvent, respectively, η the solvent viscosity and a the sphere radius. Here, p is the latex volume fraction at close packing and k a numerical constant, which are determined to have the values of 0.58 and 5.4, respectively.

Although the above equations can be used for data fitting, they do not adequately provide useful insight into the sedimentation process in terms of hydrodynamical forces or particle distribution. In this regard, more detailed theories are needed. Two such theories are discussed below.

Pairwise Hydrodynamical Interactions

A convenient starting place for quantitative analysis of the sedimentation problem lies in the solution of the Navier-Stokes Equations, first derived by Navier in 1827.[23] These equations, along with the appropriate boundary conditions, provide the velocity distribution of fluid for flow around a given shaped object. Since spheres are convenient objects, the problem is most suitably formulated for such particles. Unfortunately, the fluid velocity for a sphere of radius a falling at a speed of v_{Stokes} varies asymptotically as $v_{Stokes}(a/r)$, where r is the radial distance from the sphere[24]. This dependence makes summing the effects from all spheres falling in a dispersion divergent. In 1971, G. K. Batchelor[24] devised a way in which the integrals involved would not be divergent and was thus able to solve for the sedimentation velocity of the dispersion.

The prescription employed, which ignores Brownian motion and inertial forces on either the particles or fluid and carried out for only statistically homogeneous dispersions of monodisperse hard spheres, is as follows. The average velocity of a settling sphere is written as,

$$\overline{\mathbf{v}}_{part} = \frac{1}{N!} \int \mathbf{v}(\mathbf{x_o}, \Im_N) P(\Im_N \mid \mathbf{x_o}) d\Im_N \tag{9}$$

where $\mathbf{v}(\mathbf{x_o}, \Im_N)$ is the velocity of a test sphere with its center at $\mathbf{x_o}$, N is the number of spheres and $P(\Im_N \mid \mathbf{x_o})d\Im_N$ the probability of a configuration of N sphere centers being found in the range $d\Im_N$ about $\Im_N$ given there is a sphere center at $\mathbf{x_o}$. $\Im_N$ is the set of position vectors of the centers of N spheres in one configuration. It is the dependence of the velocity $\mathbf{v}(\mathbf{x_o}, \Im_N)$ on other surrounding spheres which causes the above integral to diverge. Considering hydrodynamical interactions between groups of no more than two spheres, Batchelor was able to

rewrite Eq. 9 in a nondivergent form. Note that Eq. 9 represents the average veloctiy of a sphere in the solvent fixed frame. It so happens that when Batchelor evaluates the nondivergent form of this equation, the reference frame of choice is the volume fixed reference frame. Thus, his result is immediately expressible in a form comparable to experiment. His calculations yield a sedimentation velocity of

$$v = v_{Stokes}(1 - 6.55\phi)$$

thus placing the suspicions of previous empirical relations on a more firm theoretical foundation. However, since only pairwise hydrodynamical interactions were included, the results are limited to dilute suspensions of $\phi \leq 0.05$. To extend to higher volume fractions, full N-body hydrodynamical interactions must be included. To achieve this, another approach may be used.

Full N-body Hydrodynamical Interactions

In 1984, Beenakker and Mazur[18] calculated the short time, wavevector dependent diffusion coefficient valid for systems of hard, monodisperse spheres at volume fractions up to $\phi = 0.45$. In their formulation, full N-body hydrodynamical interactions are included in the construction of the equations. However, spatial correlations are taken only at a pairwise level in evaluating the result. The N-body hydrodynamical interactions included in Beenakker and Mazur's equations allow for the calculation of the diffusion constant up to high volume fractions.

Using a relation between the diffusion coefficient at zero wavevector and the isothermal compressibility of the suspension, one may obtain the sedimentation velocity of the spheres in the volume fixed reference frame. The resulting analysis of these calculations are compared to experiment in Chapter V.

CHAPTER III

SAMPLES

Materials

The "hard" particles used in these studies are 0.99μm diameter polymethylmethacrylate (PMMA) spheres with a relative standard deviation less than 0.05, sterically stabilized with an approximately 10nm thick coating of poly-12-hydroxylstearic acid and suspended in a mixture of decahydronapthalene (decalin) and 1,2,3,4 tetrahydronapthalene (tetralin). The PMMA has an index of refraction of 1.51, decalin 1.47 and tetralin 1.54. By mixing the decalin and tetralin in a ratio chosen to closely match the index of refraction of the particles, the resulting suspensions can be made nearly transparent, even up to volume fractions (ϕ) greater than 0.70. If the samples were not index matched, they would appear milk white and opaque to visible light. It has been observed that a drift from index matching occurs on the order of weeks after initial matching of the suspension. We have tried to minimize this drift by using particles which have previously been index matched. However, our samples would not index match to near transparency. The best which could be achieved were samples with a slight yellow opacity, whose clarity increased to near transparency during the course of the experiment. One reason for this may be due to slow tetralin adsorbtion onto the stabilizing layer. Water contamination of the tetralin is another possible explanation for the discoloration. Two small vials were filled with approximately equal amounts of tetralin and decalin, both containing a small amount of water. After allowing the vials to set for a couple of months, the yellow discoloration was noticed in the vial containing tetralin, but none in the decalin vial. A similar occurance may be present in the PMMA samples as the air enclosed with the sample at the time of sealing

may contain moisture, resulting in contamination of the sample. The effect of this tetralin discoloration on density and index of refraction is presumed negligible and was not considered in further analysis of data. The specification sheets for tetralin note the color as ranging from clear to yellow tinted when purchased. The steric stabilizing layer consists of large polymer molecules chemically bound to the surface of the particles. There are two effects due to these molecules which keep the particles from flocculating. One is the volume restrictive effect. As the particles approach one another, the polymer molecules begin entangling. This reduces the number of available configurations for the molecule and thus leads to an increase in the free energy of the particle-particle pair. Also, since the region between the particles increases in polymer molecule concentration, osmotic effects may cause the solvent to diffuse into this area forcing the particles apart, although this only will occur in a "good" solvent for the stabilizing layer.

Preparation

Initially PMMA particles were partially index matched in a solvent mixture of tetralin and decalin and collected in a single jar where large debris was allowed to sediment. The colloidal liquid was then decanted into four $\sim$ 25ml vials and centerfuged. The clear supernatant was decanted and the four vials were concentrated into two. To further clean and characterize the samples, they were centrifuged, decalin decanted and new decalin which had been filtered through a 0.2μm MILLEX-FG filter added to the concentrate and the samples remixed to a liquid. This process was repeated three times to ensure filtered decalin as the particle environment. These two vials were then transfered to another two, preweighed vials, again centrifuged, decalin decanted and the resulting vials containing randomly packed sediment weighed. These samples have a volume fraction of particles $\phi = 0.637$ in decalin and serve as a possible check of the volume fraction determintaion. Tetralin and decalin was added to each vial, index matching the resulting suspensions as best as could be achieved.

By keeping track of the original PMMA and decalin weights in the preweighed vials, along with the weight of tetralin added to index match the suspension, the individual component weights can be calculated. This was achieved via vacuum oven drying (100C° for ~4hrs) a weighed amount of index matched sample from one of the two vials. The two vials were then mixed together in a larger, preweighed distribution bottle, again index matched, and another sample taken and dried in a similar fashion. From the wet and dry sample weights, the weight fraction of PMMA spheres to solvent can be determined. These wet and dry sample weights, along with knowing how much tetralin has been added through out the index matching process, allow for the determination of individual PMMA, decalin and tetralin component weights. The above process was complex and not the best way to determine volume fractions. In retrospect, drying and weighing a given amount of sample which has been taken from a single collection bottle containing only PMMA and one solvent (i.e. decalin) is much more convenient than the method described above. One, then knowing the PMMA to decalin weight fraction, only needs to keep track of the weight of tetralin added to the bottle when index matching, in order to calculate all of the constituent component weights in the suspension.

Samples ranging in volume fraction of particles from $\phi = 0.42$ to $\phi = 0.60$ were made by the centrifugation of 5cc cuvettes filled with index matched sample from the distribution bottle and the removal of clear supernatant to achieve the target volume fractions. Knowing the relative solvent weights, one can calculate the weight of solvent needed to be decanted in order to obtain the correct volume fractions. The samples were simply set on a Sartorius digital balance capable of measuring $1x10^{-4}$g and the appropriate solvent weight pippeted out. The cuvettes were tumbled to redisperse the particles, tightly capped and sealed with teflon tape to avoid solvent evaportation and left to stand at room temperature (22C° $\pm$ 1C°) for a period of two months. A minimal amount of careful movement was required for periodic weighing which was performed to keep record of the rate of solvent evaporation. Note that once the dispersion has settled far enough so that

a clear supernatant develops, there is effectively no change of the volume fraction which characterizes the samples. Since this condition occurred within six days for even the most concentrated sample, decalin and tetralin evaporation can be considered negligible over the course of the experiment. If the samples are remixed for subsequent sedimentation studies, then the evaporation loss must be considered in the determintation of the initial sample volume fraction.

CHAPTER IV

SETTLING EXPERIMENTS

Sedimentation Height Measurements

The sedimentation heights of the various levels were measured via a telescopic eyepiece, vertical translating stage and incandescent backlighting as shown in Fig. 1. The resolution of the vernier on the translation stage is 0.005cm and the telescope contained a horizontal retical which allowed for easy locating of any vertical level within the sample cell. All heights were measured relative to the inside bottom of each cuvette.

If one allows the samples to set undisturbed, after about one day, distinct layers will become visible in each. These interface heights may be plotted as a function of time as is shown in Fig. 2 for four samples of increasing volume fraction. Six distinct regions may be identified which describe the sedimentary phases observed within the samples: (A) clear supernatant, (B) colloidal liquid, (C) polycrystalline solid, where the bulk colloidal liquid has nucleated crystallites which begin sedimenting, (D) high density polycrystalline solid and (E) columnar crystal sediment which occurs in low volume fraction samples, and (F) a phase which appears amorphous or glassy. Clear supernatant (A) is the solvent mixture depleted of any PMMA spheres and has a volume fraction of zero. Colloidal liquid (B) is the mixture of solvents and spheres, and is presumed to have a volume fraction maintained at the original value when the sample was initially mixed, except for a narrow region at the B/C interface where a density gradient may develope. In the polycrystalline solid phase (C) the PMMA spheres have coalesced into discrete crystallites within the colloidal liquid. Crystallite formation can easily be observed

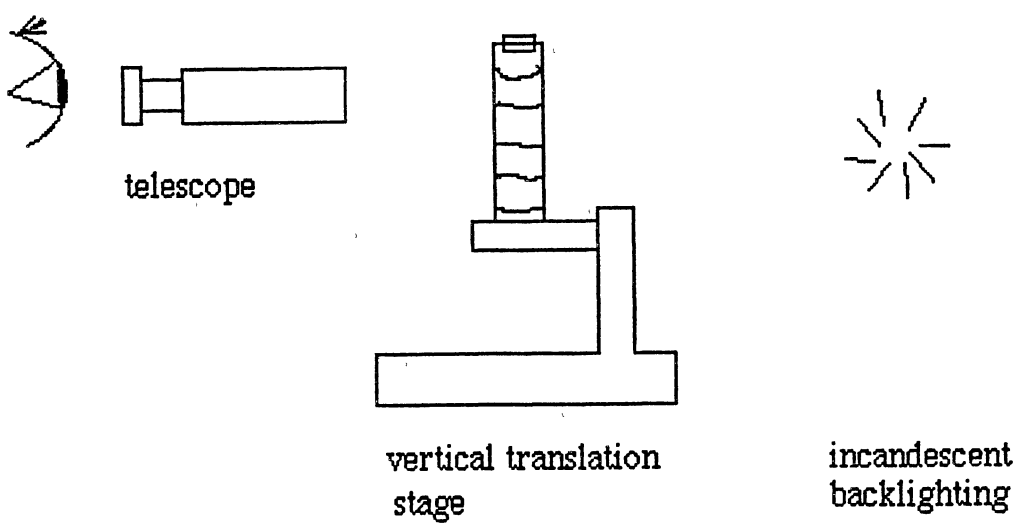

Figure 1. Experimental set-up for sedimentation height measurements.

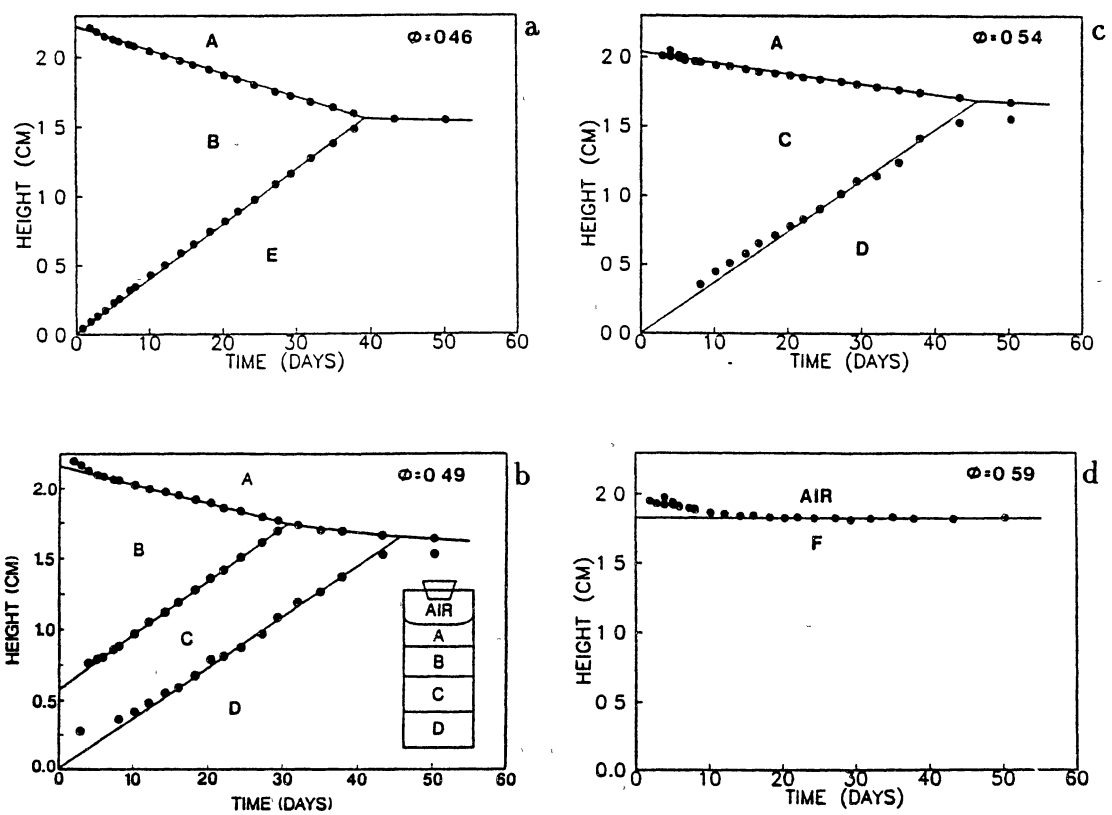

Figure 2. Sedimentaion height versus time for several samples of increasing volume fraction. Here (A) is clear supernatant, (B) colloidal liquid, (C) polycrystalline solid, (D) high density polycrystalline solid (E) columnar crystal sediment and (F) amorphous or glassy phases.

in this region as brightly colored specks within the bulk liquid, these specks being due to Bragg scattering from localized regions of spatial order formed by the crystallites. These crystallites, if the suspension is sufficiently dilute, sediment into there own region, leaving colloidal liquid above. If the sample is sufficiently concentrated, the sample will be fully crystalline with a clear supernatant region above. High density polycrystalline sediment (D) is polycrystalline solid which has settled to the bottom of the cuvette and is further sedimenting. The volume fraction of this region is found to be less than closest packing for hard spheres, due to the random settling of individual crystallites which may not fit together in closest packed formation and/or due to compressive distortion of the crystal microstructure. If the sedimentation of spheres occurs at a rate slow enough, as it does for these colloidal liquids, diffusive processes enable the migration of the spheres into close packed structures. These grow from the bottom of the cuvette in a phase in which there appears to be an ordering of the sediment into rising columnar regions (E). Above this columnar crystal sediment is colloidal liquid (B) or ultimately clear supernatant. If the sample is highly concentrated, the sample appears amorphous or glass-like (F) in nature throughout the entire sample volume. There is no formation of crystallites nor is there any significant sedimentation.

All samples investigated contained at least one or a combination of these six layers, depending upon the initial volume fraction which determines where the sample lies within the phase diagram shown by Fig. 3. Here (L) corresponds to liquid, (C) coexisting liquid and crystal, (X) fully crystalline and (G) glass phases, respectively. The four figures shown in Fig. 2 depict the height versus time diagrams corresponding to these four regions of the phase diagram. In the liquid phase, Fig. 2a, region (C), (D), and (F) are not present as the only crystal structures which form are columnar. Samples in the coexistence region, Fig. 2b, evidence four regions, (A)→(D), the dense polycrystalline solid replacing the columnar crystal of lower volume fraction samples. In fully crystalline samples, Fig. 2c, region (B) is negligible and presumed to be caused by shear melting when weighing and regions (E) and (F) not present. The glass phase, region (F) shown in Fig. 2d,

produces no distinct boundaries and the sample is amorphous or glassy, failing to crystallize, except for a small region at the very top, during the time scale of the measurements. Further sedimentation measurements were extended to $\phi = 0.099$ by successive dilutions of one of the samples ($\phi = 0.415$).

In Fig. 2a and b, the initial nonlinearity in the A/B boundary results from the curvature of the air/sample miniscus. On the other hand, the nonlinear behavior of the B/C interface is due to the sedimentation of the crystallites which initially formed within the bulk colloidal liquid. These crystallites initially sediment until phase separation of polycrystalline solid and colloidal liquid occurs, at which point the B/C interface begins to rise due to the nucleation of new crystallites at the interface. It is believed this region of spontaneous nucleation to be very narrow as no particle density gradient was visually observed throughout the experiment. For completeness, height versus time data from all other samples has been included in appendix B.

Finally, we observe columnar crystal growth and no dense amorphous sediment for $\phi^* < \phi_f^*$, while the computer simulations of microsphere sedimentation by Russel and Davis[15] produce mixed crystal and amorphous sediments for samples of similar volume fraction and Peclet number, in agreement with experiments on silica suspensions. This difference indicates the possibility of experimental polydispersity in particle size in the silica systems or a lack of hardness in the PMMA spheres used in this work.

Phase Diagram

A phase diagram, Fig. 3, is constructed by extrapolating the linear portion of the height versus time boundaries to zero time. In this limit only crystal (C) and/or liquid (B) regions exist, regions (A), (D), (E) and (F) having extrapolated to zero volume. Thus the crystal fraction may be determined unambiguously and should correspond to that in the absence of settling. The diagram presents the percent crystal versus volume fraction ϕ. The freezing and melting points are found to be $\phi_f = 0.477$ and $\phi_m = 0.533$, respectively, using a linear regression fit to the

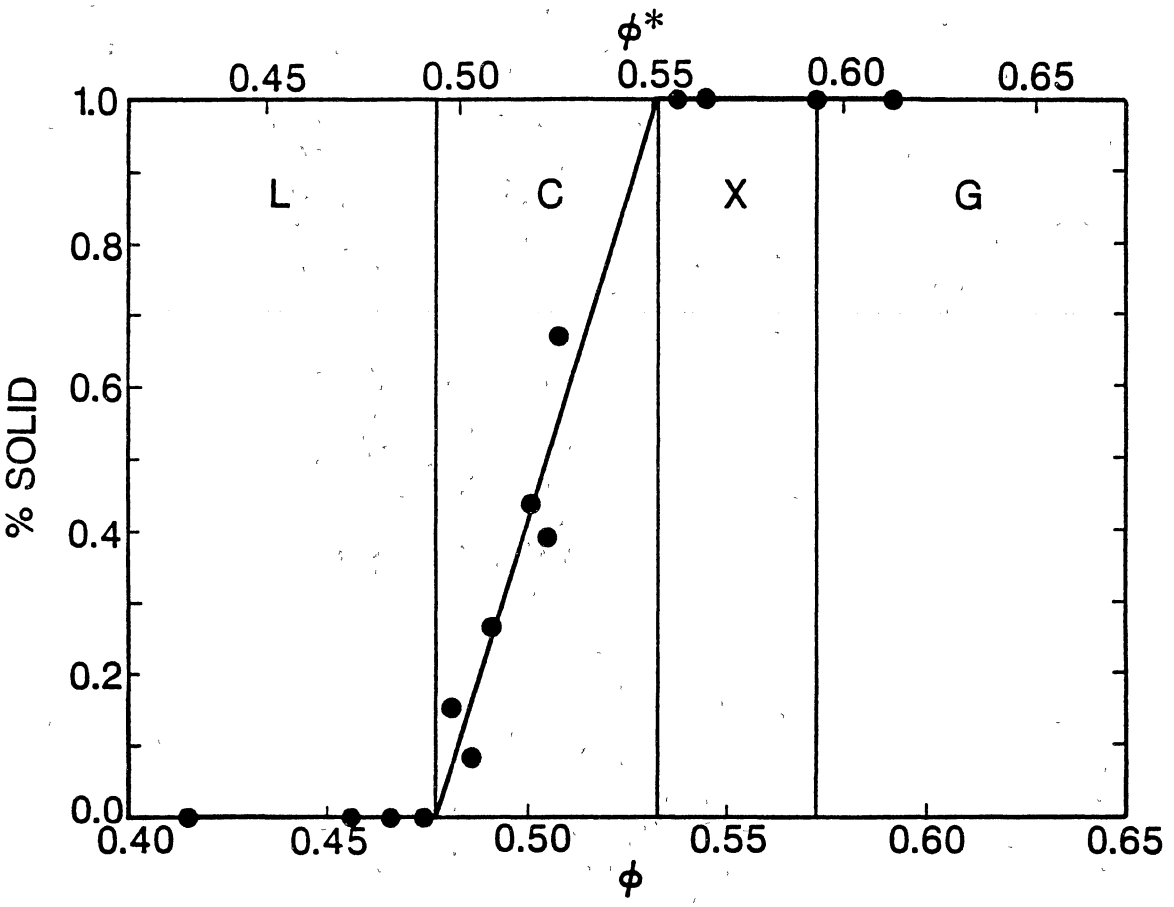

Figure 3. Phase diagram obtained from samples. Scaled and measured volume fractions are shown on the upper and lower horizontal axis, respectively. (L) is liquid, (C) coexistence, (X) crystal, and (G) glass phases, respectively.

coexistence region data. The results for hard sphere phase behavior, determined by computer simulations[1], give the freezing and melting volume fractions to be 0.494 and 0.545, respectively. The lack of agreement with our results indicates a possible increase in particle size due to adsorbtion of the solvent onto the stabilizing layer, which is not included in the dry weight determination of ϕ, or to a deviation from true hard sphere interactions.[8] Pusey and van Megen[8] have observed a larger discrepancy for smaller diameter particles having the same steric stabilizer but suspended in decalin and CS_2. To account for possible solvent adsorbtion and to compare with hard sphere theory, they scale the measured volume fraction to coincide with the theoretical hard sphere freezing point. Following this same procedure the volume fractions presented here are scaled using $\phi^* = (0.494/0.477)\phi$ as shown by the upper horizontal axis of Fig. 3. It is interesting to note that this corresponds to an effective radius increment for the particles of only $\sim$ 6nm. Our scaling is 4% while Pusey and van Megen's correction was of the order of 20% and is consitent with having a thinner stabilizing layer relative to the particle diameter. This indicates the spheres used in these samples as being a closer approximation of hard spheres.

Sedimentation Velocities

Sedimentation velocities of the liquid and crystal are calculated from the linear regions of the boundary lines shown in Fig. 2. For the colloidal liquid $\phi^* < \phi_f^*$ and for the fully crystalline samples, the sedimentation velocity is given directly by the slope of the uppermost boundary A/B and A/C, respectively. For the coexistence region the colloidal liquid sedimentation velocity is determined as above and the crystal sedimentation velocity is determined from the B/C boundary using particle conservation and the melting and freezing crystal densities ϕ_f^* and ϕ_m^*, respectively. Once a sample in the coexistence region phase seperates into colloidal liquid and crystalline regions, the falling colloidal liquid phase nucleates and grows new crystallites at the B/C boundary. This produces a rise in the B/C boundary with time. At the same time there is a slower sedimentation of the

polycrystalline solid which produces a fall in the B/C boundary with time. It is this rate of sedimentation we wish to obtain via knowing the velocity of the falling A/B boundary and the net *rising* B/C boundary, quantities we can measure.

Consider the mass of colloidal liquid (B) of density ρ_l, passing through a hypothetical horizontal plane of area A with a velocity v_l in a time Δt. The change in mass is

$$\Delta M_L = A v_l \rho_l \Delta t. \tag{10}$$

Now, consider the mass of polycrystalline solid (C) of density ρ_c passing through a similar hypothetical plane of area A with a speed v_c during the same time interval. Here the change in mass is

$$\Delta M_C = A v_c \rho_c \Delta t. \tag{11}$$

Provided $\Delta M_L > \Delta M_C$, the difference between Eq. 10 and Eq. 11 gives the amount of mass, ΔM, built up at the B/C boundary during the time interval Δt,

$$\Delta M = A(v_l \rho_l - v_c \rho_c)\Delta t \tag{12}$$

Experimentally, the B/C boundary is observed to propagate upward with a velocity v. One may write the amount of colloidal liquid (B) being converted into polycrystalline solid (C) during a time interval Δt as $Av\rho_l\Delta t$. Likewise, the mass of new polycrystal one observes gained during this time interval is $Av\rho_c\Delta t$. Thus the amount of mass built up at the B/C boundary during the interval Δt is the difference between how much new polycrystalline solid (C) is generated and how much colloidal liquid (B) was converted,

$$\Delta M = A(\rho_c - \rho_l)v\Delta t. \tag{13}$$

Equating Eq. 12 and Eq. 13, and solving for v_c results in,

$$v_c = \frac{\phi_l}{\phi_c}(v_l + v) - v$$

where $\rho_l/\rho_c = \phi_l/\phi_c$. The crystal sedimentation velocity has also been estimated from the slope of the A/C boundary after the region B has completely sedimented

into C. While there is general agreement with the two estimates of the sedimentation velocity, the height versus time data for the A/C boundary is limited and evidenced a larger variation.

The measured sedimentation velocities are normalized to the sedimentation rate of an isolated sphere (given by Eq. 8), giving the reduced sedimentation velocity K= v_{meas}/v_{Stokes}, which is plotted in Fig. 4 as a function of ϕ^*. The solvent viscostiy, η, used in calculating v_{Stokes} was experimentally determined to be 2.28x10$^-$3Pas @ 22°C using a Bohlin Constant Stress Rheometer. In Fig. 5, for $\phi_f^* < \phi^* < \phi_m^*$, two reduced sedimentation velocities are shown at each ϕ^* value measured. The upper corresponds to the liquid phase and the lower to the crystalline phase. That is, it is seen that the sedimentation rates of the colloidal liquid and polycrystalline phases are independent of ϕ^*. Because sedimentation velocities are a function of volume fraction and in the coexistence region the colloidal liquid and polycrystalline volume fractions are fixed at ϕ_f^* and ϕ_m^*, respectively, this ϕ^* independent sedimentation velocity region should be expected. This observation serves as a marker for the phase transition and could be used in other systems to confirm or establish a phase transition when other measurements are not easy or possible. Furthermore, the phase diagram is used to define the liquid ϕ_f^* and solid ϕ_m^* volume fractions uniquely. For $\phi^* \geq \phi_m^*$ the reduced sedimentation velocity corresponds to that for the polycrystalline solid phase. The $\phi^* = 0.59$ and 0.61 points correspond to glass samples which never crystalized during the period of observation.

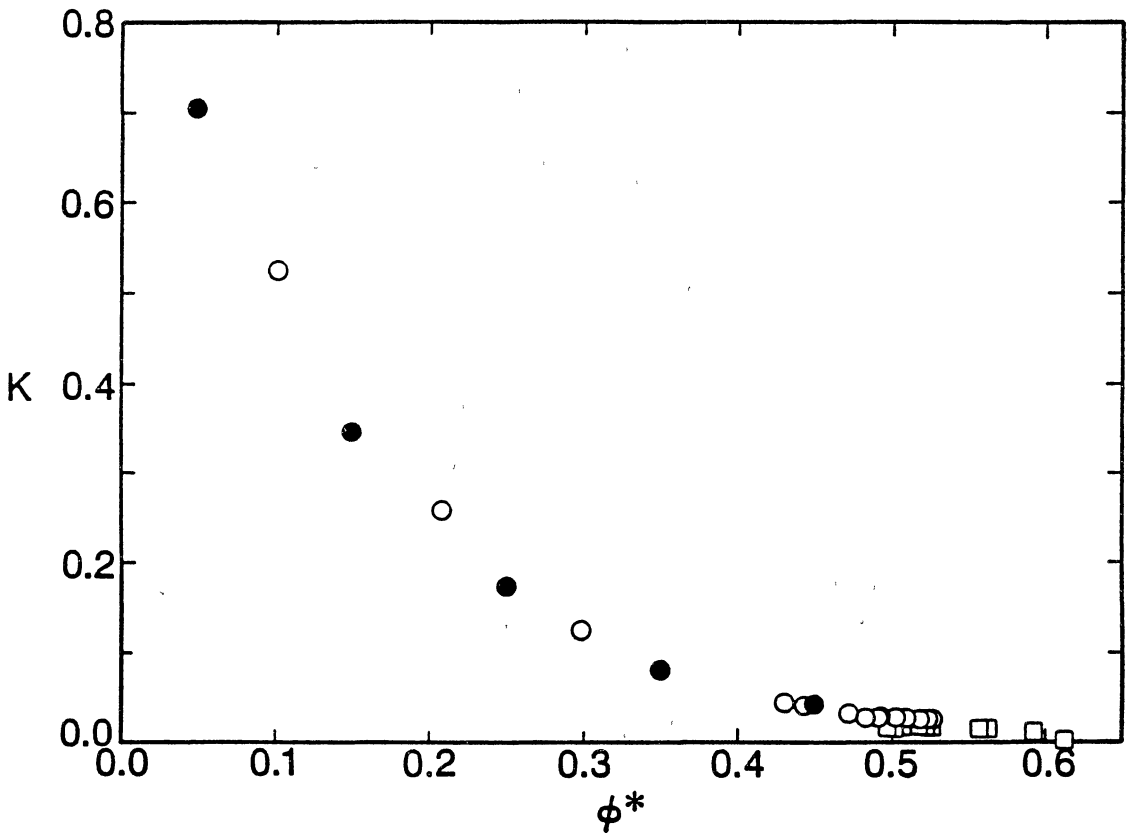

Figure 4. The reduced sedimentation velocity from experimental data for liquid (○) and crystal (□) is shown. The theory of Beenakker and Mazur (●).

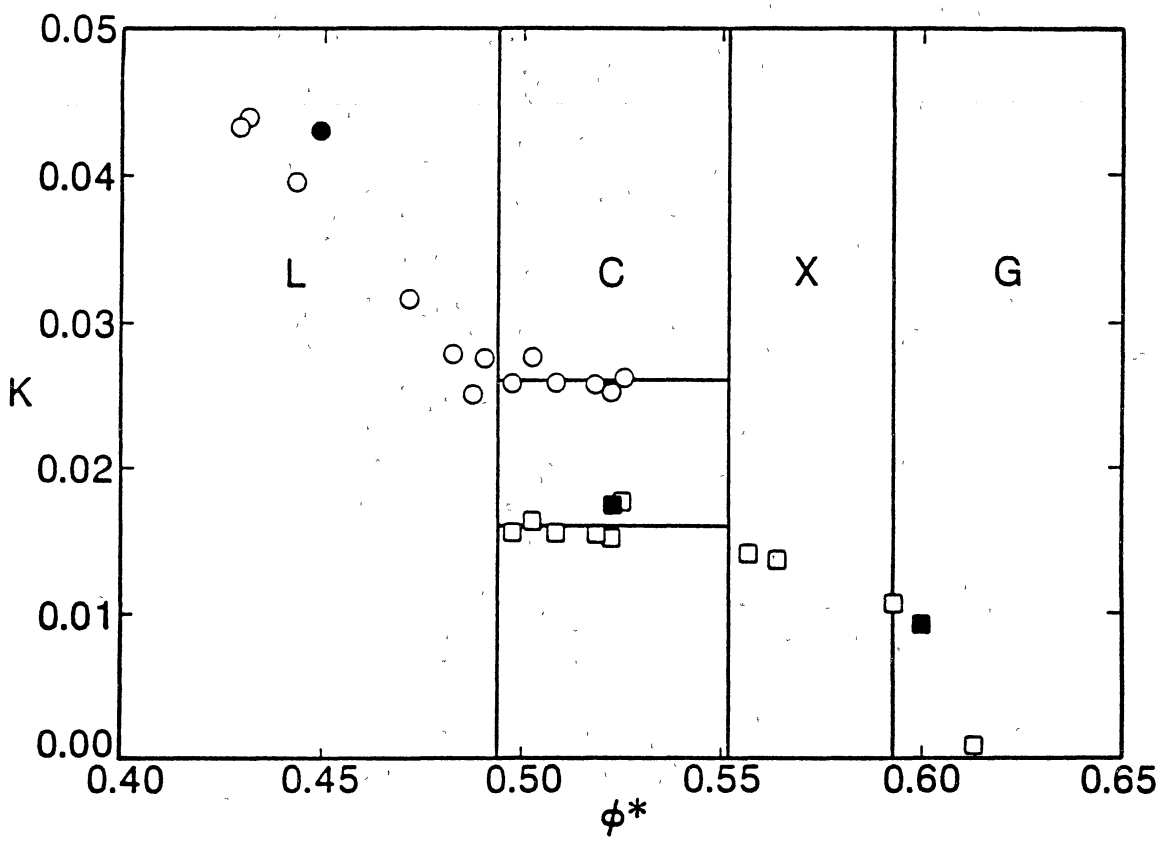

Figure 5. Close-up of the transition region with the theory of Zick and Homsy (■). (L) is liquid, (C) coexistence, (X) crystalline and (G) glass regions.

CHAPTER V

EMPIRICAL AND THEORETICAL COMPARISON

A number of empirical formulas have been presented to correlate settling data for hard spheres.[19]-[21] Only relatively recently have more rigorous microscopic theories been developed.[16,18] However, the many body nature of the hydrodynamic interaction ultimately necessitates using approximations to calculate the reduced sedimentation velocity. In Fig. 4, for $\phi^* < \phi_f^*$, the data is compared with the theoretical results of Beenakker and Mazur.[18] In this theory N-body hydrodynamic interactions are included with spatial correlations taken only at a pairwise level in evaluating the result. Furthermore, a form for the sedimentation velocity is used which neglects memory function effects. Thus "zero g" equilibrium particle distribution functions are assumed for evaluation of any ensemble averages. Despite these approximations the comparison with this and other data is quite good. For $\phi^* > \phi_f^*$ in the polycrystalline phase, the data may be compared with calculations of the hydrodynamic resistance of a rigid, oriented, single crystal structure.[28,29] In Fig. 5 the results of Zick and Homsy[28] for an FCC crystal with the [100] direction parallel to the average flow are shown. The agreement with experimental data is again seen to be quite good despite the samples being randomly oriented, polycrystals having a close packed random stacked order. Furthermore, the particles are not constrained to fixed lattice positions. In this regard, Saffman has shown in dilute suspensions that thermal motion and response to flow can have significant effect.[30] Because the cuvettes are stationary in time, the experimental measurements obtained here are by their nature in a volume fixed frame. It should be noted that the theories of Zick and Homsy and of Beenakker and Mazur are calculated in the volume fixed reference frame, so no reference frame corrections have been necessary to compare theory with experiment. A note of thanks is in

order to J. F. Brady for useful discussions with Dr. Ackerson concerning reference frames and the above theories.

Fig. 6 compares the experimental data of this work with the "hard sphere" work of others for $\phi^* < \phi_f^*$. Although the other authors data are for silica in cyclohexane[11] and polystyrene latex in $1x10^{-3}$ mole dm^{-3} sodium chloride solution[21], the agreement is good. Both model their data with hard sphere interparticle potentials.

A copy of a Physical Review Letter summarizing the above work has been included in appendix A.

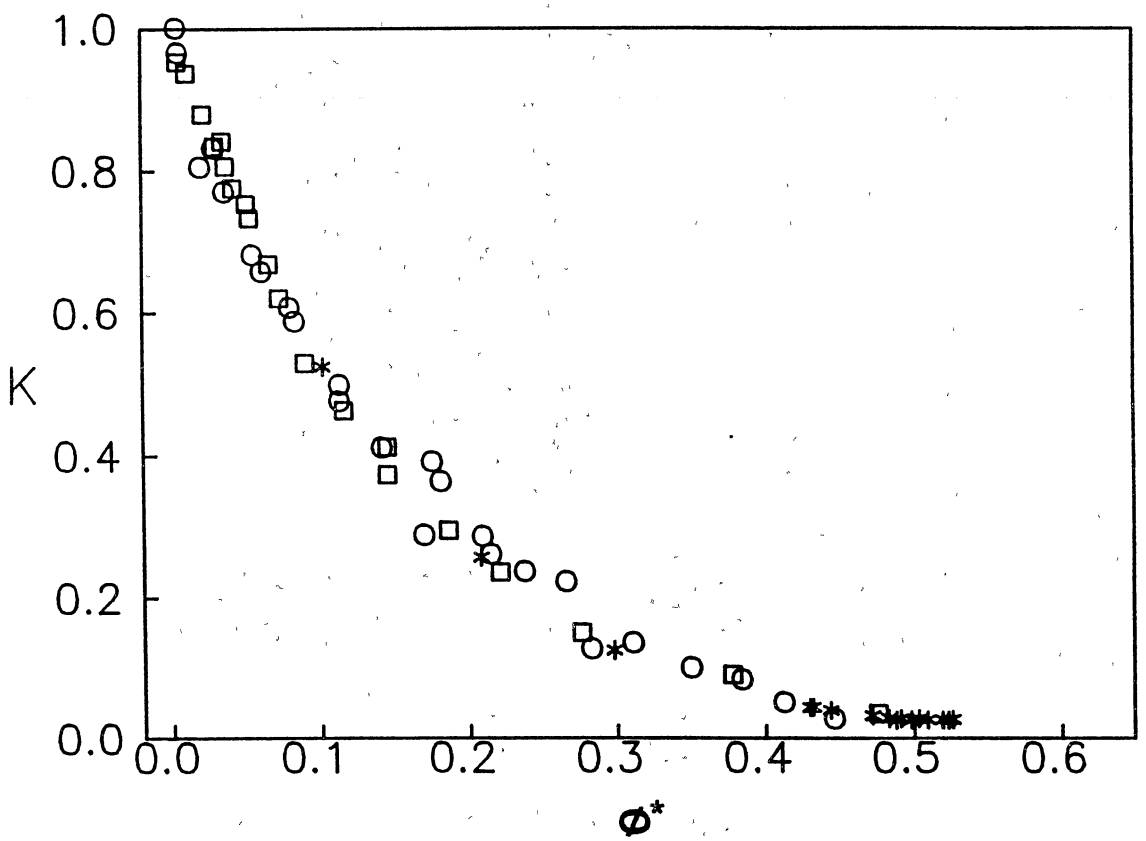

Figure 6. Comparison of reduced sedimentation velocity data with experimental data of other authors for ϕ_f^*. ($*$) this work, (○) Kops-Werkhoven and Fijnaut, and (□) Buscall et. al..

CHAPTER VI

SCATTERING MEASUREMENTS

Although the five layers (A)→(E) have been visually tracked over a period of time, one would like to know more detailed information about the individual layers themselves. i.e. what are their density and how uniform is that density throughout a given layer? In particular, such measurements have been made for regions of polycrystalline solid, high density polycrystalline solid and columnar crystal sediment. Regions (C), (D) and (E) of Fig. 2, respectively.

A 15mW beam from a HeNe laser was made incident upon a sample of interest and the resultant scattering imaged on a frosted screen placed 4.85cm directly in front of the sample. Fig. 7 depicts a schematic drawing of such an arrangement. The images are then digitized utilizing a G. W. Hannaway and Associates image processing system and placed in a frame buffer for further enhacement. The scattering pattern observed is an annular ring speckeled with bright spots. The cause of this speckled ring is randomly oriented crystallites which satisfy the Bragg condition. From the radius of this ring the volume fraction of the individual crystallites may be calculated. The scattering is assumed to be from the [111] planes of crystallites with FCC structure, or equivalently from the stacked planes of crystallites constructed of hexagonal close packed layers. One may notice from Fig. 7 that scattering from crystallites at the front and back walls of the cuvette will give the scattering ring a characteristic width. An average ring radius has been calculated for both the vertical and horizontal ring widths and the scattering assumed localized from the center of the cuvette in any subsequent analysis of data.

Assuming an FCC structure, the volume occupied by the spheres in the crystal unit cell is $4V_{sphere}$, where V_{sphere} is the volume of a single sphere. The

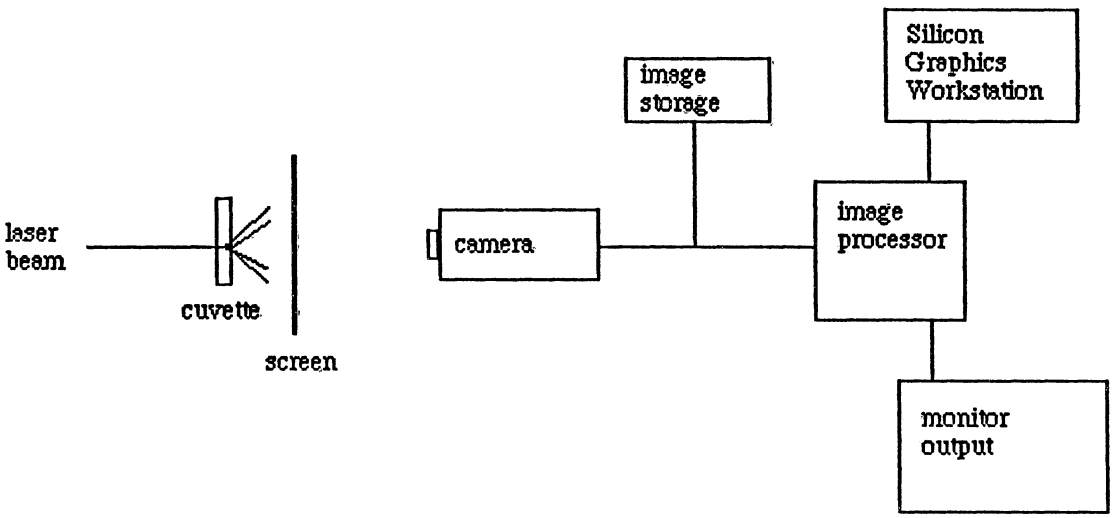

Figure 7. Experimental set-up for light scattering measurements showing image capture and storage capability.

volume of the unit cell is j^3, where j is the second neighbor distance. This results in a volume fraction of $4V_{sphere}/j^3$ for a single crystallite. Following the scattering geometry of Fig. 8, the volume fraction of the crystallite can be calculated as a function of scattering ring radius provided j can be expressed as a function of R. One can write Bragg's Law for first order scattering as

$$\frac{\lambda}{n'} = 2t \sin \frac{\theta'}{2} \tag{14}$$

where λ is the wavelength of incident radiation, n' the index of refraction of the decalin and tetralin solvent mixture and t the lattice spacing of the [111] planes. The lattice constant, t is related to the second neighbor distance as,

$$t = \frac{j}{\sqrt{3}} \tag{15}$$

thus, using Eqs. 14 and 15, one may write,

$$j = \frac{\sqrt{3}\lambda}{2n' \sin(\frac{\theta'}{2})}. \tag{16}$$

Using Snell's Law

$$n \sin\theta = n' \sin\theta', \tag{17}$$

and the geometry of Fig. 8, one may show

$$R = a \tan\theta' + d \tan[\sin^{-1}(\frac{n'}{n} \sin\theta')]. \tag{18}$$

If Eq. 18 could be inverted and an expression for θ' as a function of R derived, one could, using Eq. 16, achieve the desired result. However, due to the difficulty of inverting of Eq. 18, data for R as a function of θ' was calculated for a range of R values coincident with experimental observation ($R \sim$ 6.5cm to 4.2cm) and a polynomial fit to third order, with R as the independent variable obtained, giving an empirical equation of θ' as a function of R. This, combined with Eq. 16 enable j to be calculated as a function of R and thus the crystallite volume fraction as a function of scattering ring radius, R. This, of course, assumes isotropic compression of the crystals

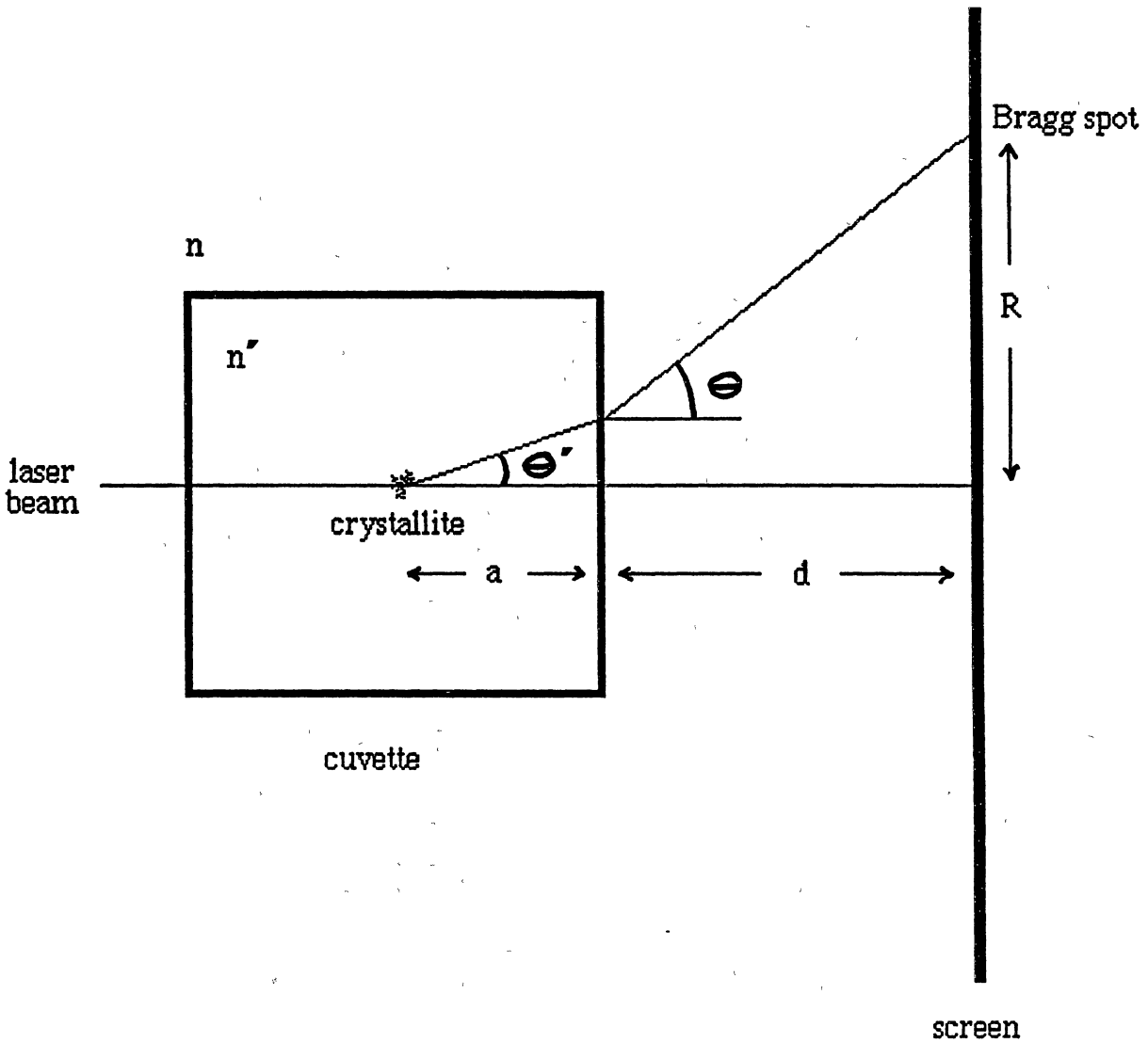

Figure 8. Diagram depicting Bragg scattering from a crystallite in the cuvette to the imaging screen. Here n and n′ are the indices of refraction of the air and sample, respectively, a+d the distance of the crystallite from the screen and R the scattering ring radius.

Figs. 9 and 10 depict the volume fraction for crystallites formed in samples in regions of columnar crystal (E), and the transition from polycrystalline solid (C) to dense polycrystalline solid (D), respectively. Here the calculated crystallite volume fraction is plotted as a function of sample height . Profiles for several days have been placed on each plot so that the B/E or C/D boundary, Figs. 9 and 10, respectively may be tracked over a period of time. The important feature noted in all three diagrams is the anisotropy of the crystallite volume fraction in the vertical and horizontal directions. This difference corresponds to $\sim$ 2% compression on the [111] lattice spacings in the vertical direction. This anisotropy of the crystal structure casts doubt on the above derivation for crystallite volume fraction and is a point of needed attention and interest in future work. Density profiles for all other samples are included in appendix C.

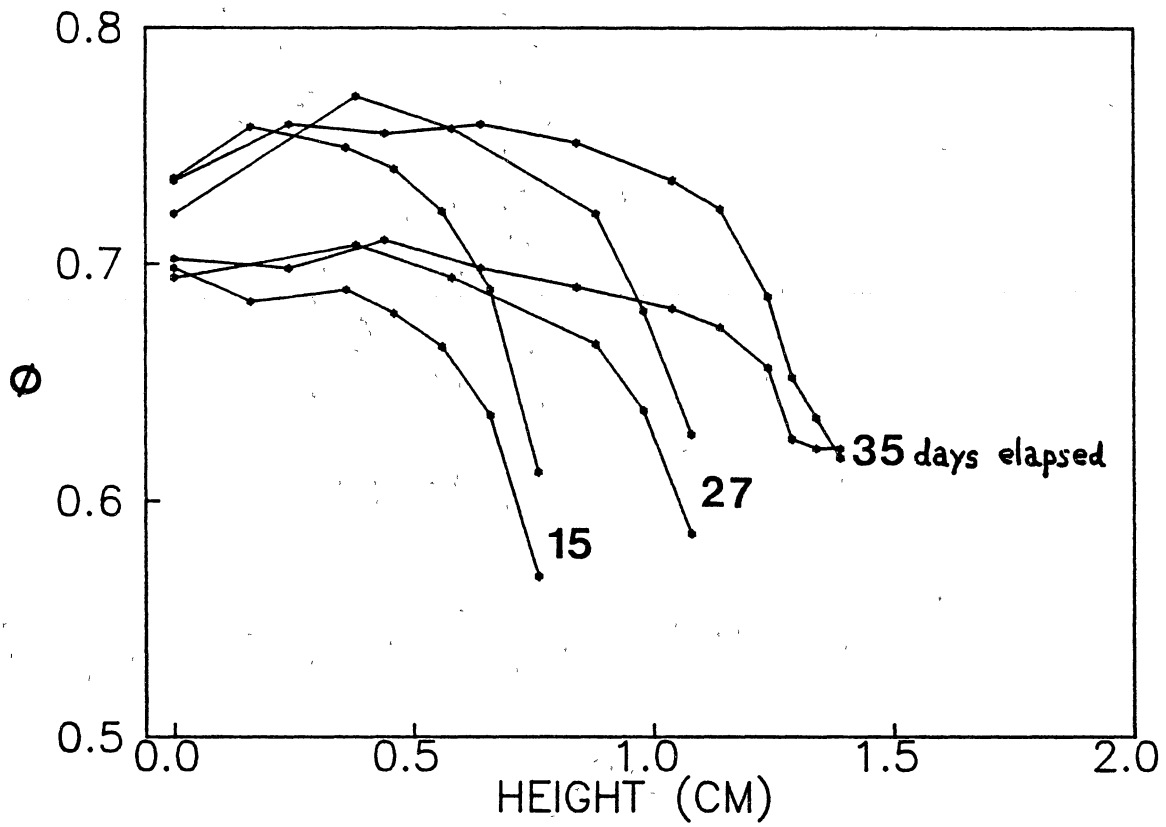

Figure 9. Density profiles obtained from light scattering measurements over a period of $\sim$ three weeks. This figure corresponds to scattering from the columnar crystal region, (E) of a sample in the liquid region of the phase diagram. Here $\phi = 0.47$.

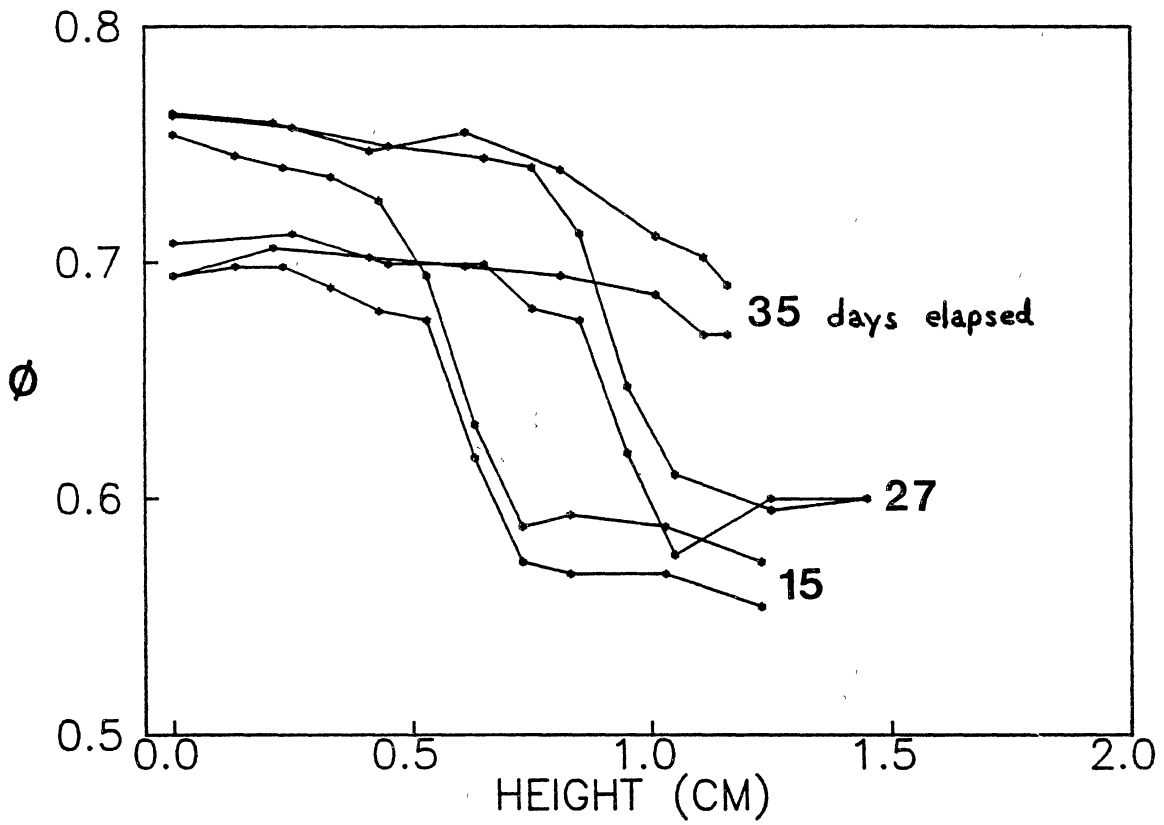

Figure 10. Density profiles obtained from light scattering measurements over a period of $\sim$ three weeks. This figure corresponds to scattering from the polycrystalline and dense polycrystalline regions, (C) and (D), respectively, of a sample in the coexistence region of the phase diagram. Here $\phi = 0.49$.

CHAPTER VII

CONCLUSIONS

In this work, sedimentation velocities have been experimentally determined for suspensions of nearly hard polymethylmethacrylate spheres as a function of volume fraction. In addition to this, a brief discussion of scattering data has been included. These results are important in further characterizing colloidal PMMA systems and in presenting a connection between hard sphere sedimentation theory and experiment. In this regard, the preceeding work has been benificial in establishing a precident for observing the freezing/melting transition in the reduced sedimentation velocity, $K(\phi^*)$, for a system of "hard" spheres and using the equilibrium phase transition as a unique marker for the volume fraction in concentrated systems. These values are found to be $K(\phi_f^*) = 0.026$ and $K(\phi_m^*) = 0.016$.

The anisotropy of the crystal structure in the dense polycrystalline sediment (D) regions is an area of needed work in the future, both in terms of experimental rigor and physical understanding of the formed structures. Here, questions are open as to whether the compressed phase is in equilibrium or even how to incorporate the anisotropy into the calculation of crystallite volume fraction.

BIBLIOGRAPHY

[1] B. J. Alder, W. G. Hoover and D. A. Young, J. Chem Phys. **49,** 3688 (1968).

[2] B. B. Laird, J. D. McCoy and A. D. J. Haymet, J. Chem. Phys. **87,** 5549 (1987).

[3] E. Thiele, J. Chem. Phys. **39,** 474 (1963).

[4] Norman F. Carnahan and Kenneth E. Starling, J. Chem. Phys. **51,** 635 (1969).

[5] J. A. Barker and D. Henderson, Ann. Rev. Phys. Chem. **23,** 439 (1972).

[6] J. D. Weeks, D. Chandler and H. C. Andersen, J. Chem. Phys. **54,** 5237 (1971).

[7] R. Zwanzig, J. Chem. Phys. **22,** 1420 (1954).

[8] P. N. Pusey and W. van Megen, *Complex and Supermolecular Fluids* Wiley-Interscience, New York (1987).

[9] C. G. de Kruif, P. W. Rouw, J. W. Jansen and A. Vrij, J. de Physique **46,** C3-295 (1985).

[10] J. W. Jansen, C. G. de Kruif and A. Vrij, J. Colloid Int. Sci. **114,** 501 (1986).

[11] M. M. Kops-Werkhoven, C. Pathmamanoharan, A. Vrij and H. M. Fijnaut, J. Chem. Phys. **77,** 5913 (1982).

[12] M. M. Kops-Werkhoven and H. M. Fijnaut, J. Chem. Phys. **74,** 1618 (1981).

[13] M. M. Kops-Werkhoven and H. M. Fijnaut, J. Chem. Phys. **77,** 2242 (1982).

[14] G. K. Batchelor, J. Fluid Mech. **74,** 1 (1976).

[15] K. E. Davis and W. B. Russel, Adv. in Ceramics **21,** 573 (1987).

[16] John F. Brady, Ronald J. Phillips, Julia C. Lester and Georges Bossis, J. Fluid Mech. **195,** 257 (1988).

[17] B. Cichocki and B. U. Felderhof, Physica A **154,** 213 (1989).

[18] C. W. J. Beenakker and P. Mazur, Physica A **126,** 349 (1984).

[19] A. D. Maude and R. L. Whitmore, British J. of Appl. Physics **9**, 477 (1958).

[20] C. C. Reed and John L. Anderson, AIChE J. **26**, 816 (1980).

[21] R. Buscall, J. W. Goodwin, R. H. Ottewill and Th. F. Tadros, J. Colloid Int. Sci. **85**, 78 (1982).

[22] K. E. Davis, W. B. Russel, and W. J. Glantsching, Science, **245**, 507 (1989).

[23] J. Happel and H. Brenner, *Low Reynolds Number Hydrodynamics,* Prentice-Hall, Englewood Cliffs, N.J. (1965).

[24] G. K. Batchelor, J. Fluid Mech. **52**, 245 (1971).

[25] P. N. Pusey and W. van Megen, Nature (London) **320**, 340 (1986) and Phys. Rev. Lett. **59**, 2083 (1987).

[26] Bruce J. Ackerson and P. N. Pusey, Phys. Rev. Lett. **61**, 1033 (1988).

[27] J. -C. Bacri, C. Frénois, M. Hoyos, R. Perzynski, N. Rakotomalala and D. Salin, Europhys. Lett. **2**, 123 (1986).

[28] A. A. Zick and G. M. Homsy, J. Fluid Mech. **115**, 13 (1982).

[29] H. Hasimoto, J. Fluid Mech. **5**, 317 (1959).

[30] P. G. Saffman, Studies in Appl. Math. **102**, 115 (1973).

APPENDIXES

APPENDIX A

COPY OF PHYSICAL REVIEW LETTER IN WHICH SEDIMENTATION RESULTS ARE PUBLISHED

VOLUME 64, NUMBER 22 PHYSICAL REVIEW LETTERS 28 MAY 1990

Observation of a Phase Transition in the Sedimentation Velocity of Hard Spheres

S E Paulin and Bruce J. Ackerson
Department of Physics, Oklahoma State University, Stillwater, Oklahoma 74078
(Received 16 January 1990)

Reduced sedimentation velocities are reported for suspensions of nearly hard PMMA (polymethylmethacrylate) spheres as a function of volume fraction The absolute sedimentation velocities are sufficiently slow compared to crystal-growth rates so that phase separation is achieved during the sedimentation process As a result the analytic behavior of the measured sedimentation velocity changes as a function of volume fraction at the freezing and melting points This transition serves as a definitive marker for comparison with theoretical predictions of sedimentation velocities for hard-sphere liquids and crystals

PACS numbers 64 60 Cn, 05 70 Fh, 64 70 Dv

The hard-sphere interaction of particles provides a simple but rich and important statistical-mechanical model of condensed matter. The melting-freezing transition has been demonstrated via molecular dynamics[1] and studied most recently via density-functional theory.[2] The liquid phase structure is modeled by the Wertheim-Thiele[3] solution to the Percus-Yevick equation, and the Carnahan-Starling equation[4] correlates the thermodynamic results of computer simulations In hard-sphere perturbation theory, many of these results are used as the basis for calculating more accurate thermodynamic properties in a perturbation expansion about the hard-sphere state [5-7] In general, these approximations are necessary because no particles interact via a true hard-sphere potential However, recently the thermodynamics and statistical properties of ideal hard-sphere systems have been used to interpret the results of experiments on colloidal suspensions of sterically stabilized particles.[8-13] These particles interact via a short-ranged repulsive interaction with the stabilizing layer mitigating any van der Waals attractive forces. Compared to the charge stabilized interactions of colloidal particles or the typical interactions of atomic particles, these interactions may prove to be the best realization of the hard-sphere potential

The nonequilibrium properties of suspended particles differ from those for purely atomic systems due to the presence of a solvent which transmits hydrodynamical forces Much theoretical work has been directed toward understanding nonequilibrium properties of model hard-sphere suspensions,[14-20] again providing a basis for understanding more complex systems having other interparticle interactions Experimental data for nonequilibrium processes in suspensions of hard spheres are limited but serve as an important check of theoretical results

In this Letter we report values for the sedimentation velocity of "hard" spheres which equilibrate locally, forming liquidlike or polycrystalline ordering of particles before significant sedimentation is observed. As a result, measurements of the sedimentation velocity have been made for randomly stacked polycrystalline phases at large volume fraction and for liquidlike phases at low volume fractions. The melting-freezing phase transition is observed in the reduced sedimentation velocity as a function of the particle volume fraction and serves as a definitive marker for comparison with theoretical results. These experimental results differ in one aspect or another from others reported for "hard"-sphere suspensions[8-13,21,22] in that our results extend to large volume fractions, the particles are not charged, and we do observe the melting-freezing transition. The failure to observe a melting-freezing transition in other work may have resulted from not having hard-sphere interactions, a polydispersity of particle size, or a sedimentation rate greater than the nucleation and growth rate for crystallites. The last condition will result in an amorphous interparticle ordering during sedimentation despite the lower free energy of the equilibrium crystal phase An order-disorder transition has been reported for the sedimentation of hard spheres,[9,22] but this is a sedimentation-induced crystallization where the increase in particle concentration on sedimentation triggers crystallization.[15]

The "hard" particles used in these studies are 0.99-μm-diam polymethylmethacrylate (PMMA) spheres having a relative standard deviation to mean radius less than 0.05, sterically stabilized with an approximately 10-nm-thick coating of poly-12-hydroxylstearic acid,[23,24] and suspended in a mixture of decaline and tetralin in a ratio chosen to closely match the index of refraction of the particles. The resulting suspensions are nearly transparent even up to volume fractions (ϕ) greater than 0.70, allowing for the visual observation of crystallite formation, the visual observation of sedimentation boundaries, and light-diffraction studies of particle microstructure. Samples ranging in volume fraction of particles from $\phi \sim 0.42$ to ~ 0.60 were made by the centrifugation of 4-cm^3 cuvettes filled with an index-matched stock sample of known sphere volume fraction and removal of supernatant to achieve the target volume fractions. For the sedimentation measurements the cuvettes are tumbled to

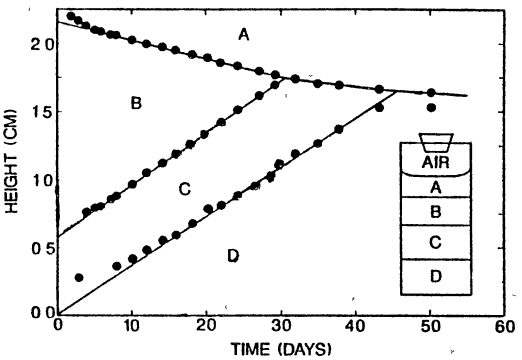

FIG 1 A representative height vs time plot of a sample with its initial volume fraction ($\phi = 0.49$) within the coexistence region A, clear supernatant, B, liquid, C, polycrystalline solid, and D, high-density polycrystalline sediment

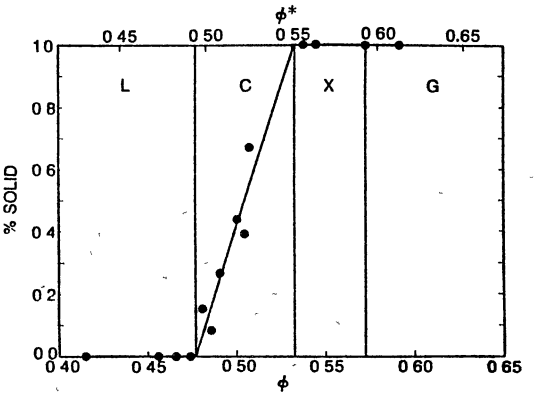

FIG 2 Phase diagram obtained from suspensions Scaled and measured volume fractions are shown on the upper and lower horizontal axis, respectively L is liquid, C coexistence, X crystal, and G glass.

redisperse the particles and left to stand a period of two months at room temperature (22 ± 1 °C), except for careful periodic weighing to monitor any solvent vapor leakage After a few days a typical sample will evidence the formation of several distinct layers as depicted in the lower right-hand corner of Fig 1. The number of layers and the particle microstructure within a layer depends on the initial volume fraction We observe four distinct types of height versus time diagrams as shown in Fig 1, corresponding to the different equilibrium phases noted in Fig. 2. Here L, C, X, and G are liquid, coexisting liquid and crystal, fully crystalline, and glass phases. The height versus time diagram in Fig 1 is typical for samples in the coexisting region, $0.477 < \phi < 0.533$ of Fig 2, where the regions are defined to be (A) clear supernatant, (B) liquid, (C) polycrystalline solid, and (D) high-density polycrystalline sediment. The volume fraction of region D for samples in the coexistence region is found to be less than closest packing for hard spheres due to the random settling of individual crystallites which may not fit together in closest-packed formation and/or due to compressive distortion of the crystal microstructure which prevents closest packing. In Fig. 1, for samples in the liquid phase, $\phi < 0.477$, region C is not present and region D shows columnar crystal growth For $0.533 < \phi < 0.573$ the samples are fully crystalline, region B being negligibly small and presumed to be caused by shear melting when weighing. For $\phi > 0.573$ there are no distinct boundaries and the sample is amorphous or glassy, failing to crystallize, except for a small region at the very top, during the time scale of our measurements Sedimentation measurements are extended to $\phi = 0.099$ by successive dilutions of one of these samples ($\phi = 0.415$). In Fig 1 the initial nonlinearity in the A/B boundary results from the curvature of the air-sample miniscus. On the other hand, the nonlinearity in the B/C boundary results from the initial nucleation and settling of crystallites throughout the entire sample.

The phase diagram in Fig 2 is constructed by extrapolating the linear portion of the layer boundaries to zero time. In this limit only crystal (C) and/or liquid (B) regions exist, regions A and D having extrapolated to zero volume. Thus the crystal fraction may be determined unambiguously and should correspond to that in the absence of settling Figure 2 presents the percent crystal versus volume fraction ϕ. The freezing and melting points are found to be $\phi_f = 0.477$ and $\phi_m = 0.533$, respectively, using a linear-regression fit to the coexistence region data. The results for hard-sphere phase behavior, determined by computer simulations,[1] give the freezing and melting volume fractions to be 0.494 and 0.545, respectively. The lack of agreement with our results indicates a possible increase in particle size due to adsorbtion of the solvent onto the stabilizing layer, which is not included in the dry-weight determination of ϕ, or to a deviation from true hard-sphere interactions.[8] Pusey and van Megen[8] have observed a larger discrepancy for smaller diameter particles having the same steric stabilizer but suspended in decalin and CS_2. To account for possible solvent adsorption and to compare with hard-sphere theory, they scale the measured volume fraction to coincide with the theoretical hard-sphere freezing point. Following this same procedure we scale our volume fractions using $\phi^* = (0.494/0.477)\phi$ as shown on the upper horizontal axis of Fig 2. It is interesting to note that this corresponds to an effective radius increment for the particles of only ~ 6 nm.

Sedimentation velocities of the liquid and crystal are

calculated from the linear regions of the boundary lines shown in Fig 1 For the liquid ($\phi^* < \phi_f^*$) and for the fully crystalline samples ($\phi_m^* < \phi^*$), the sedimentation velocity is given directly by the slope of the uppermost boundary A/B and A/C, respectively, in the height versus time diagram For the coexistence region the liquid sedimentation velocity is determined as above and the crystal sedimentation velocity is determined from the B/C boundary using particle conservation, from which one may show the velocity of the settling crystal phase to be $(\phi_f^*/\phi_m^*)(v_{mc}+v_{ml})-v_{mc}$, where ϕ_m^* and ϕ_f^* are the melting and freezing volume fractions, respectively, and v_{mc} and v_{ml} the measured boundary velocities of the B/C and A/B boundaries, respectively The crystal sedimentation velocity has also been estimated from the A/C boundary after region B has completely sedimented into C While there is general agreement with the two estimates of the sedimentation velocity, the height versus time data for the A/C boundary is limited and evidenced a larger variation

The measured sedimentation velocities are normalized to the sedimentation rate of an isolated sphere, $v_{\text{Stokes}} = 2ga^2(\rho_p-\rho_s)/9\eta$, where g is the acceleration due to gravity, ρ_p and ρ_s are the density of the sphere and solvent, respectively, η is the solvent viscosity (2.28×10^{-3} Pas at 22°C), and a is the sphere radius The reduced sedimentation velocity is given by $K = v_{\text{meas}}/v_{\text{Stokes}}$ and is plotted in Fig 3(a) as a function of ϕ^* The data for $\phi^* < \phi_f^*$, in the liquid region, agree with previous experimental results for hard spheres [13,21,25] In Fig 3(b), for $\phi_f^* < \phi^* < \phi_m^*$ two reduced sedimentation velocities are shown at each ϕ^* value measured The upper corresponds to the liquid phase and the lower to the crystalline phase It is seen that the sedimentation rates of the liquid and crystalline phases are independent of ϕ^*. Because sedimentation velocities are a function of volume fraction and in the coexistence region the fluid and crystalline volume fractions are fixed at ϕ_f^* and ϕ_m^*, respectively, these ϕ^*-independent sedimentation velocities should be expected This observation serves as a marker for the phase transition and could be used in other systems to confirm or establish a phase transition when other measurements are not easy or possible Furthermore, the phase diagram is used to define the liquid ϕ_f^* and solid ϕ_m^* volume fractions uniquely. For $\phi^* > \phi_m^*$ the reduced sedimentation velocity corresponds to that for the polycrystalline solid phase. The $\phi^* = 0.593$ and 0.613 points correspond to glass samples which never crystallized during our period of observation

A number of empirical formulas have been presented to correlate settling data for hard spheres [19–21] Only relatively recently have more rigorous microscopic theories been developed.[16,18] However, the many-body nature of the hydrodynamic interaction ultimately necessitates using approximations to calculate the reduced sedimentation velocity. In Fig 3(a), for $\phi^* < \phi_f^*$, the data are

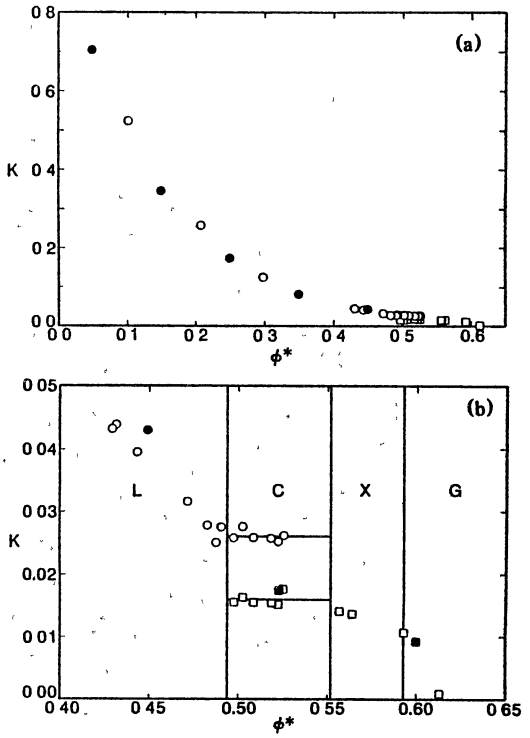

FIG 3. (a) The reduced sedimentation velocity data of liquid (○) and crystal (□) are shown as a function of scaled volume fraction with the theory of Beenakker and Mazur (Ref 18) (●). (b) Close-up of the transition region with the theory of Zick and Homsy (Ref. 26) (■), L being liquid, C coexistence, X crystal, and G glass regions

compared with the theoretical results of Beenakker and Mazur.[18] In this theory N-body hydrodynamic interactions are included with spatial correlations taken only at a pairwise level in evaluating the result. Furthermore, a form for the sedimentation velocity is used which neglects memory function effects. Thus "zero g" equilibrium particle-distribution functions are assumed for evaluation of any ensemble averages. Despite these approximations the comparison with this theory and other data is quite good. For $\phi^* > \phi_f^*$ in the crystalline phase, our data may be compared with calculations of the hydrodynamic resistance of a rigid, oriented, single-crystal structure [26,27] In Fig. 3(b) the results of Zick and Homsy[26] for an fcc crystal with the [100] direction parallel to the average flow are shown. The agreement with our data is again seen to be quite good despite our samples being randomly oriented, polycrystals having a close-

packed-random-stacked order Furthermore, our particles are not constrained to fixed lattice positions. In this regard, we note that Saffman has shown in dilute suspensions that thermal motion and response to flow can have a significant effect [28] Also, it should be noted that the data are measured and theory calculated in the same volume-fixed reference frame, and so no reference-frame corrections have been necessary to compare theory with experiment

A limited number of scattering measurements have been made from the crystal (C) and dense sedimentary (D) structures At the times when sedimentation velocities are measured, the crystal structures are uniform in density exhibiting little or no variation of density with height The dense sediment does not appear isotropic, in general, since the lattice constant in the vertical direction is -2.0% less than the lattice constant in the horizontal direction

Finally, we observe columnar crystal growth and no dense amorphous sediment for $\phi^* < \phi_f^*$, while the computer simulations of microsphere sedimentation by Davis and Russel[15] produce mixed-crystal and amorphous sediments for samples of similar reduced variables (Peclet number and volume fraction) in agreement with experiments on silica suspensions. This difference indicates the possibility of experimental polydispersity in particle size in the silica systems or a lack of hardness in our spheres In conclusion, we have measured $K(\phi^*)$ for a system of hard spheres using the equilibrium phase transition as a unique marker for the volume fraction in concentrated systems We find $K(\phi_f^*) = 0.026$ and $K(\phi_m^*) = 0.016$

We wish to thank J F. Brady and P. N. Pusey for their insightful discussions. This work is supported by U S Department of Energy Grant No DE-FG05-88ER45349.

[1]B J Alder, W G Hoover, and D A. Young, J Chem Phys 49, 3688 (1968)

[2]B B Laird, J D McCoy, and A D J Haymet, J Chem Phys 87, 5549 (1987)

[3]E Thiele, J Chem Phys 39, 474 (1963)

[4]Norman F Carnahan and Kenneth E Starling, J Chem Phys 51, 635 (1969)

[5]R Zwanzig, J. Chem Phys 22, 1420 (1954).

[6]J A Barker and D Henderson, Annu Rev. Phys Chem 23, 439 (1972)

[7]J D Weeks, D Chandler, and H C Andersen, J Chem Phys 54, 5237 (1971)

[8]P N Pusey and W van Megen, in *Complex and Supermolecular Fluids*, edited by S A. Safran (Wiley-Interscience, New York, 1987).

[9]C. G de Kruif, P W. Rouw, J W Jansen, and A Vrij, J Phys (Paris) Colloq 46, C3-295 (1985)

[10]J W Jansen, C G de Kruif, and A Vrij, J Colloid Interface Sci 114, 501 (1986)

[11]M M Kops-Werkhoven, C. Pathmamanoharan, A. Vrij, and H M Fijnaut, J Chem Phys 77, 5913 (1982)

[12]M M Kops-Werkhoven and H M. Fijnaut, J Chem Phys 74, 1618 (1981)

[13]M M. Kops-Werkhoven and H M Fijnaut, J Chem Phys 77, 2242 (1982)

[14]G K Batchelor, J Fluid Mech 74, 1 (1976)

[15]K E Davis and W B Russel, Adv Ceram 21, 573 (1987).

[16]John F Brady, Ronald J Phillips, Julia C Lester, and Georges Bossis, J. Fluid Mech 195, 257 (1988).

[17]B Cichocki and B U Felderhof, Physica (Amsterdam) 154A, 213 (1989)

[18]C W J Beenakker and P Mazur, Physica (Amsterdam) 126A, 349 (1984).

[19]A D. Maude and R L. Whitmore, Br. J Appl Phys 9, 477 (1958)

[20]C C Reed and John L Anderson, AIChE J 26, 816 (1980)

[21]R Buscall, J W Goodwin, R H Ottewill, and Th F Tadros, J Colloid Interface Sci. 85, 78 (1982)

[22]K E Davis, W B Russel, and W J Glantsching, Science 245, 507 (1989).

[23]P. N Pusey and W van Megen, Nature (London) 320, 340 (1986); Phys Rev. Lett 59, 2083 (1987)

[24]Bruce J Ackerson and P. N. Pusey, Phys Rev Lett. 61, 1033 (1988).

[25]J -C Bacri, C. Frénois, M. Hoyos, R Perzynski, N. Rakotomalala, and D. Salin, Europhys Lett 2, 123 (1986)

[26]A A. Zick and G M Homsy, J Fluid Mech 115, 13 (1982).

[27]H. Hasimoto, J. Fluid Mech 5, 317 (1959)

[28]P. G. Saffman, Stud Appl Math 102, 115 (1973)

APPENDIX B

HEIGHT VFRSUS TIME DATA FOR ALL OTHER SAMPLES

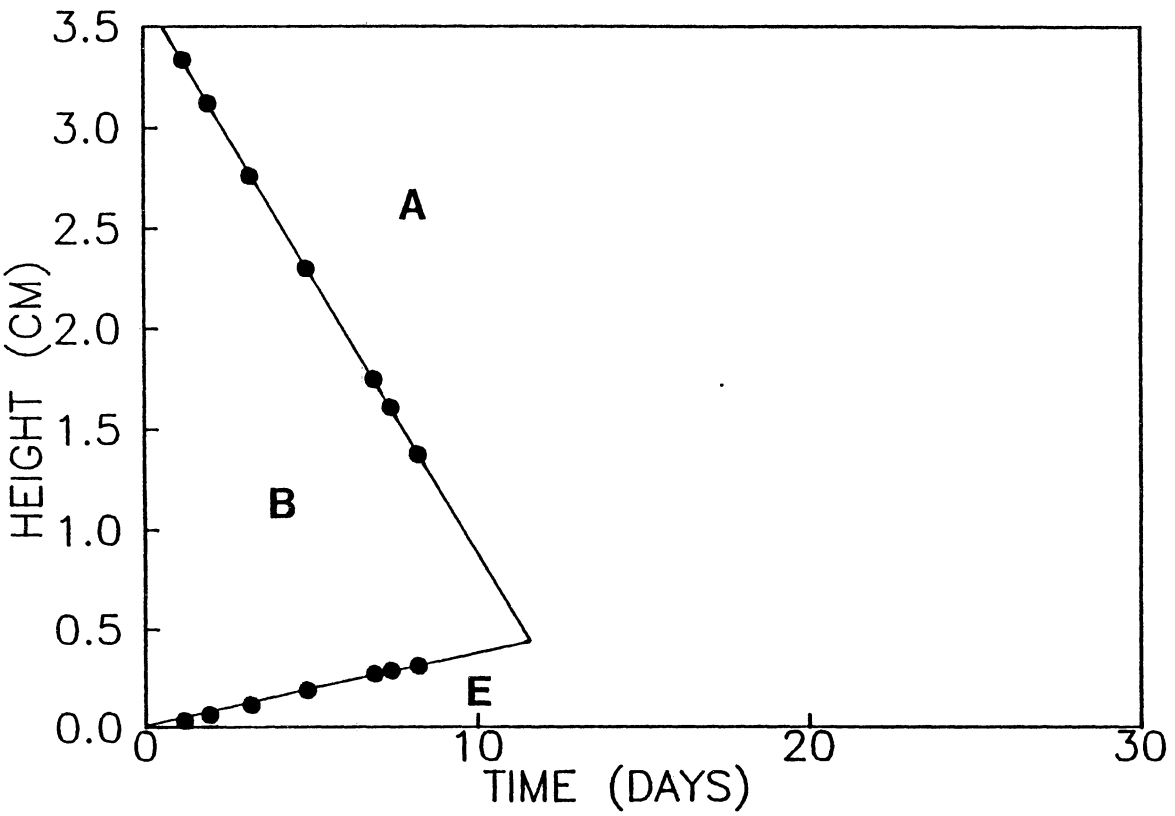

Figure 11. Sample in the liquid region of the phase diagram. $\phi = 0.099$. This is the lowest volume fraction sample observed.

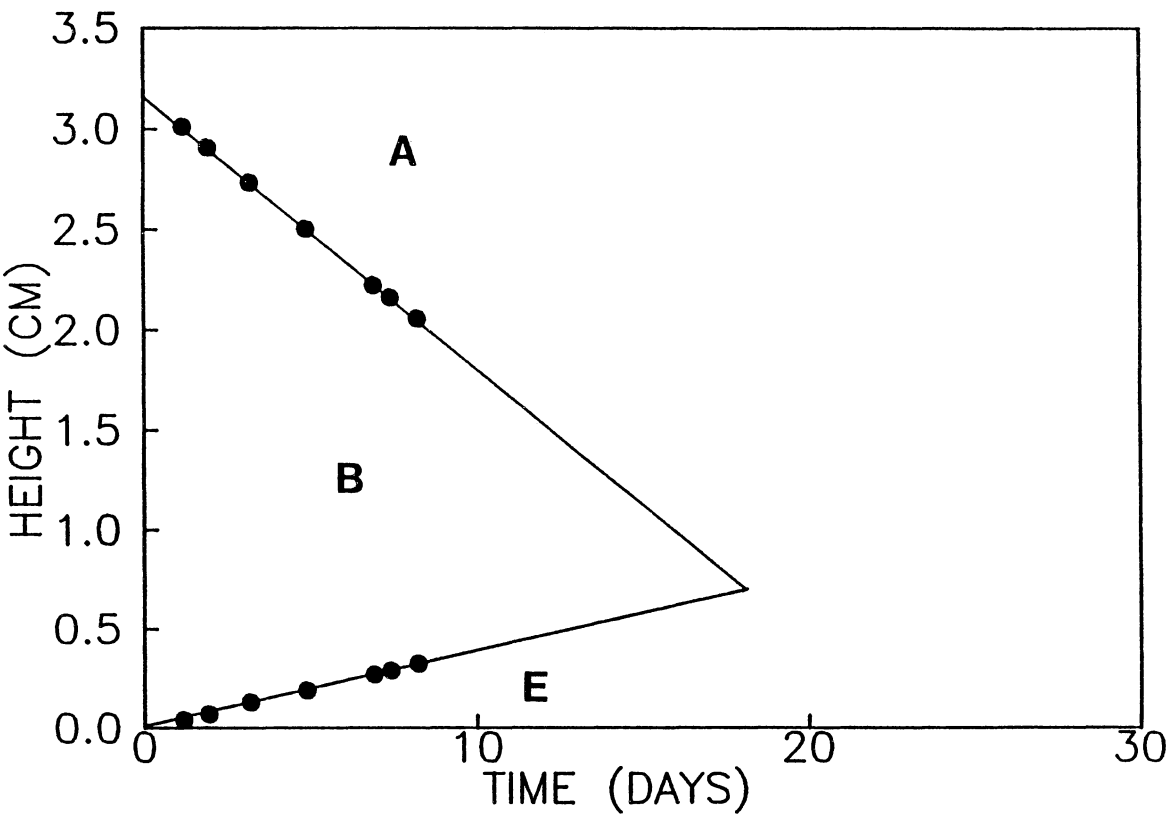

Figure 12. Sample in the liquid region of the phase diagram. $\phi = 0.20$.

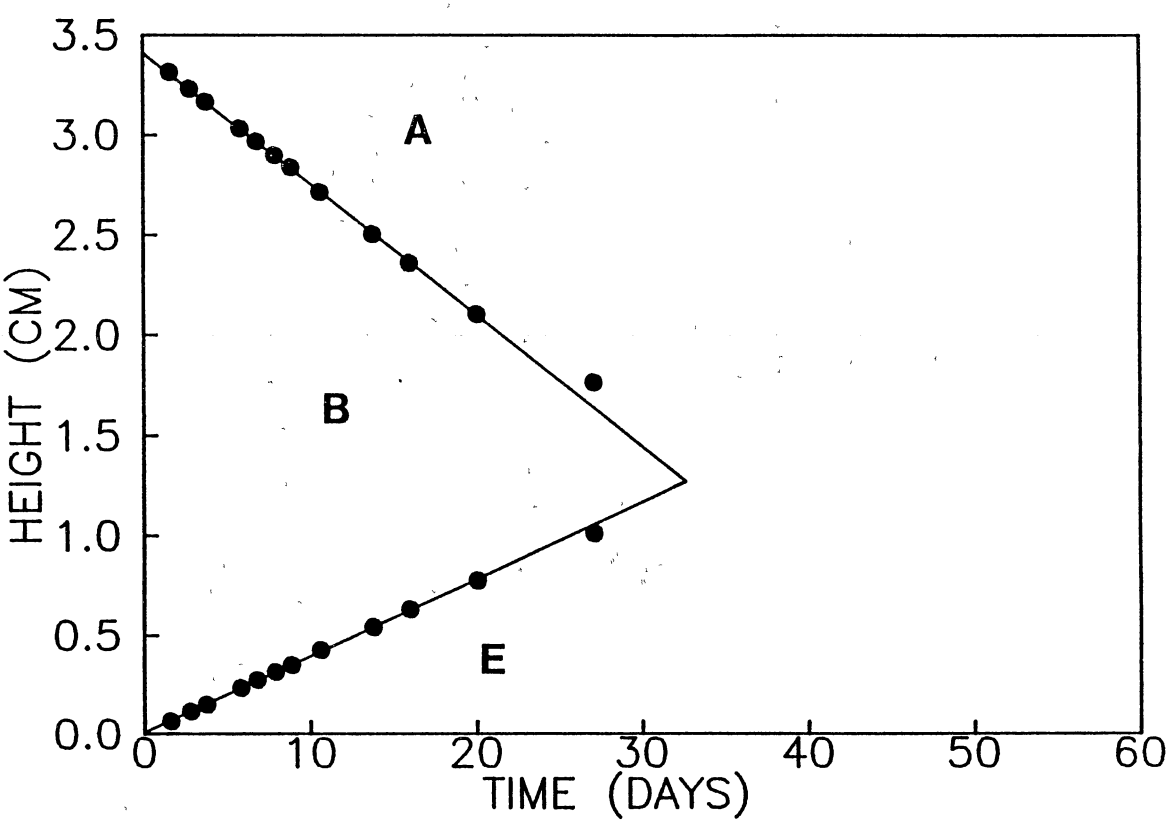

Figure 13. Sample in the liquid region of the phase diagram. $\phi = 0.29$.

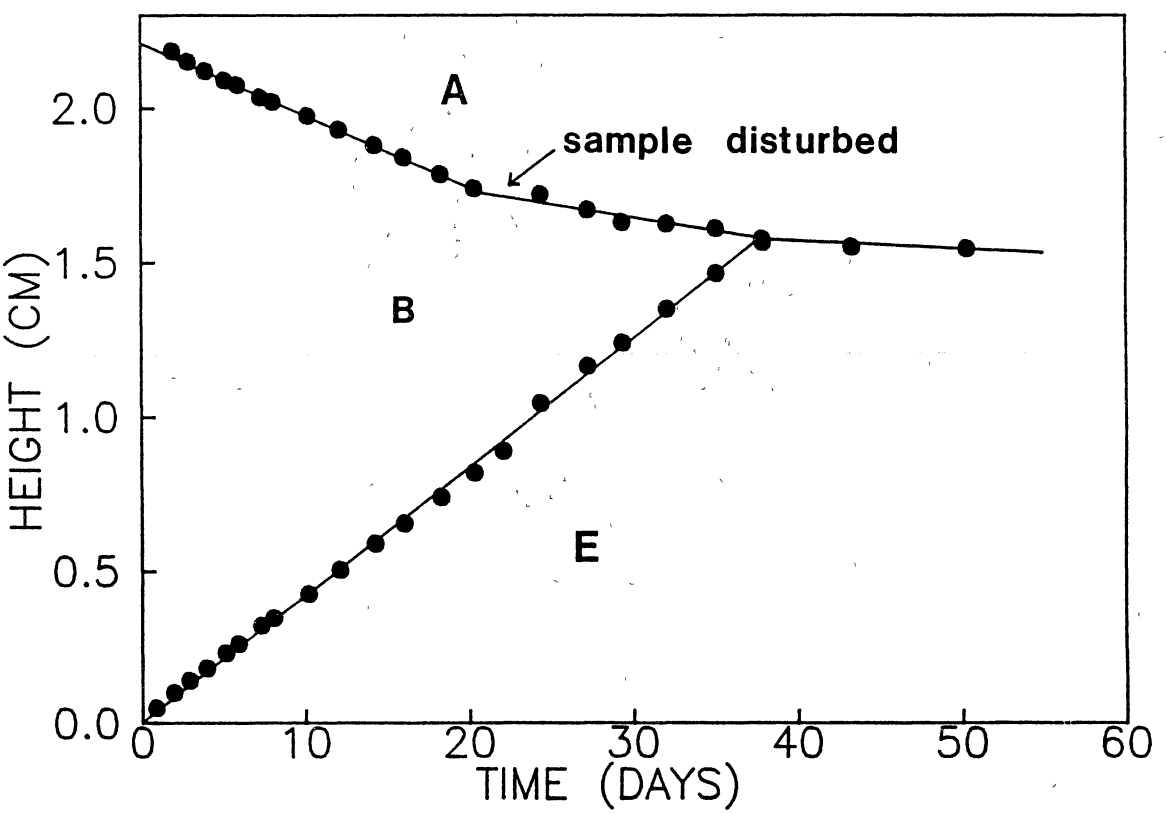

Figure 14. Sample in the liquid region of the phase diagram. $\phi = 0.42$.

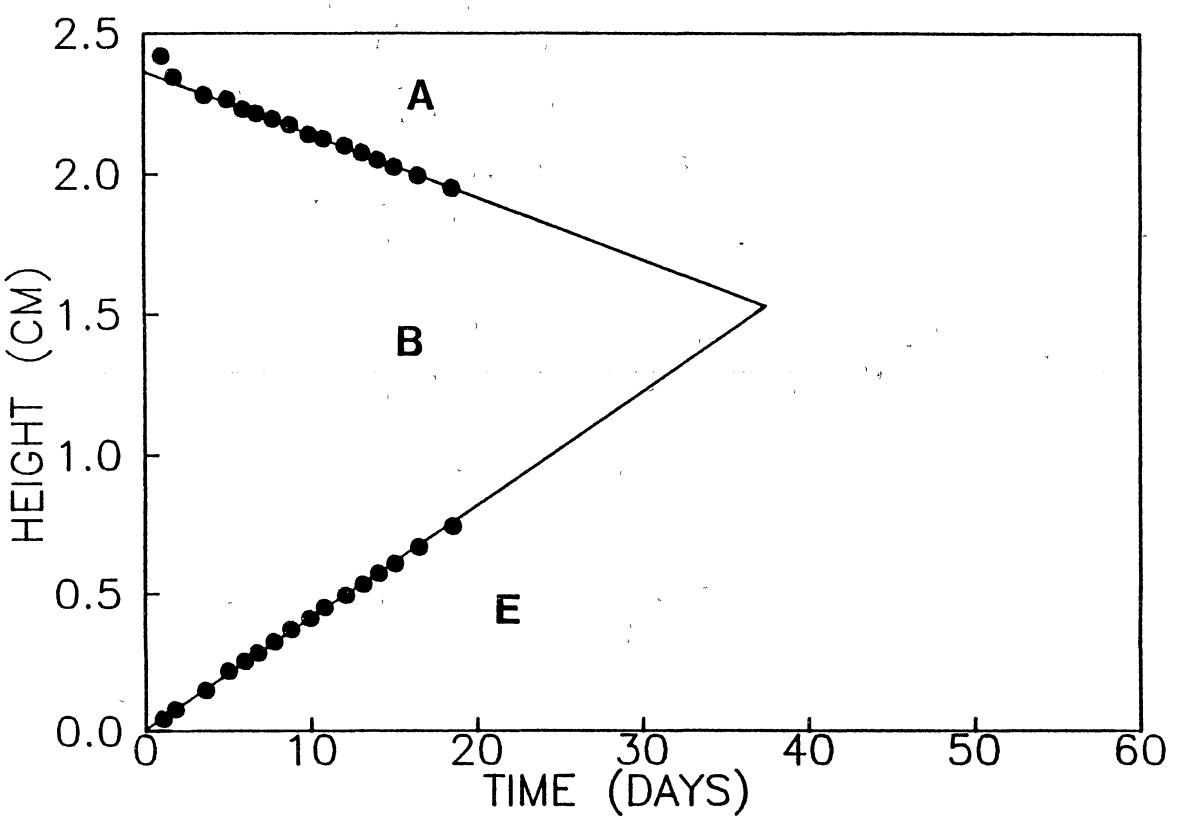

Figure 15. Sample in the liquid region of the phase diagram. $\phi = 0.42$.

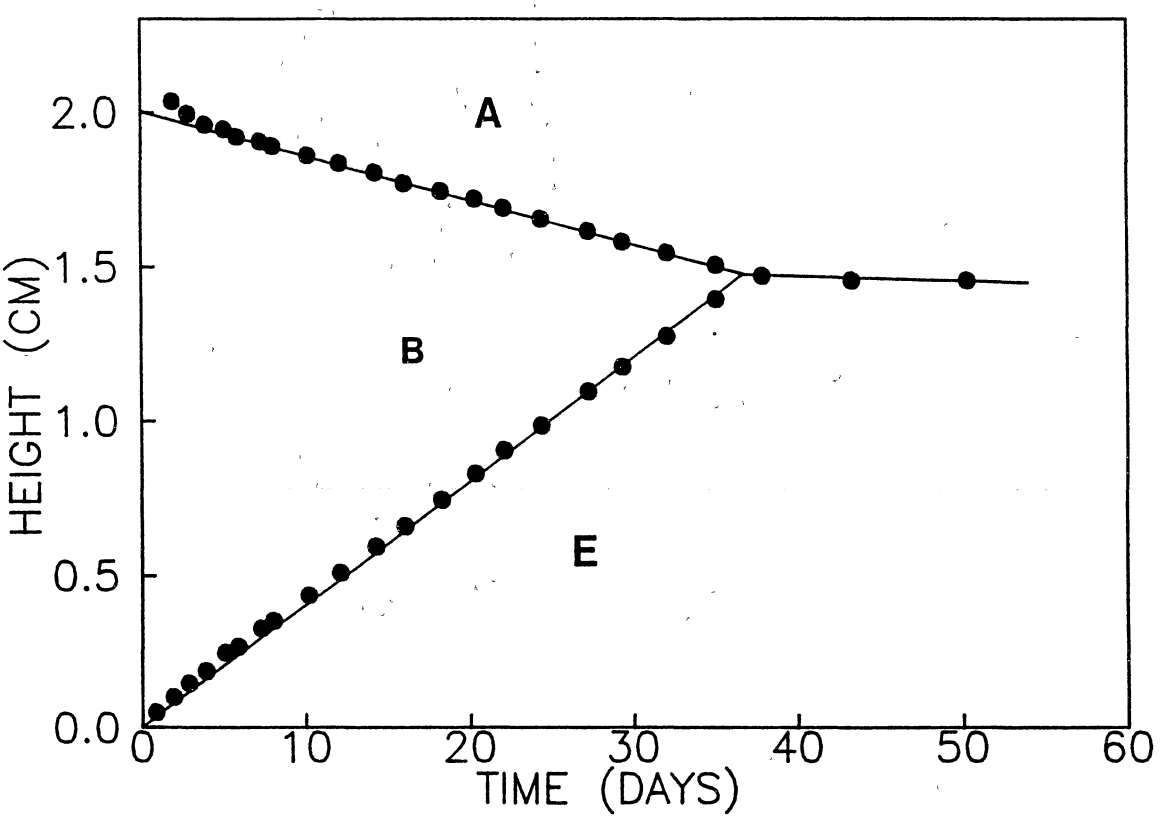

Figure 16. Sample in the liquid region of the phase diagram. $\phi = 0.47$.

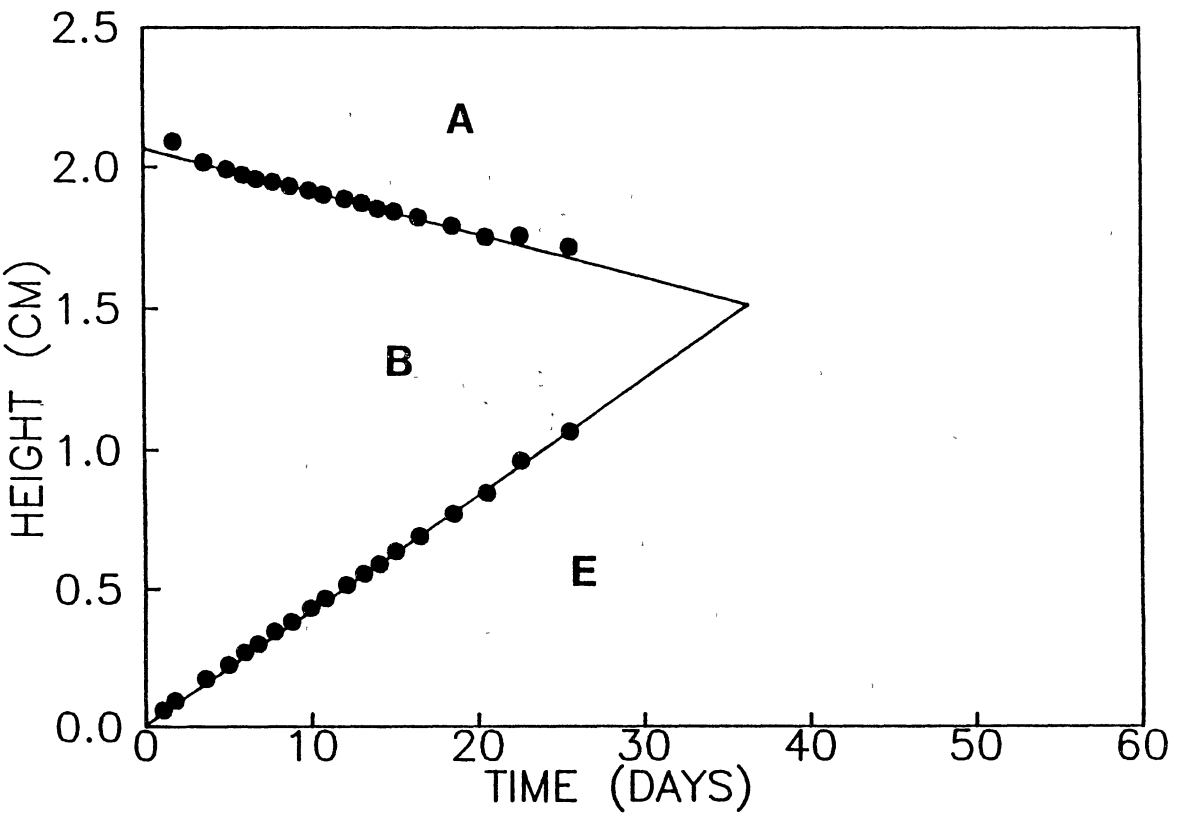

Figure 17. Sample in the liquid region of the phase diagram. $\phi = 0.47$.

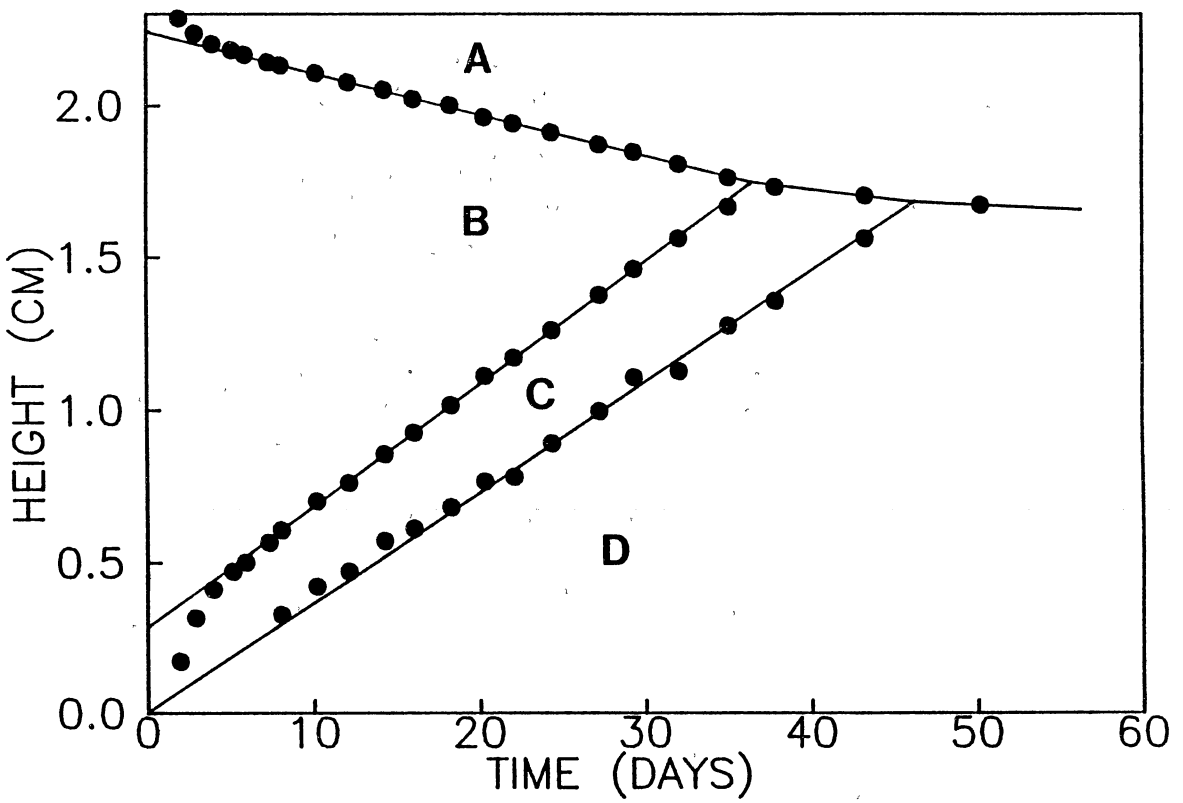

Figure 18. Sample in the coexistence region of the phase diagram. $\phi = 0.48$.

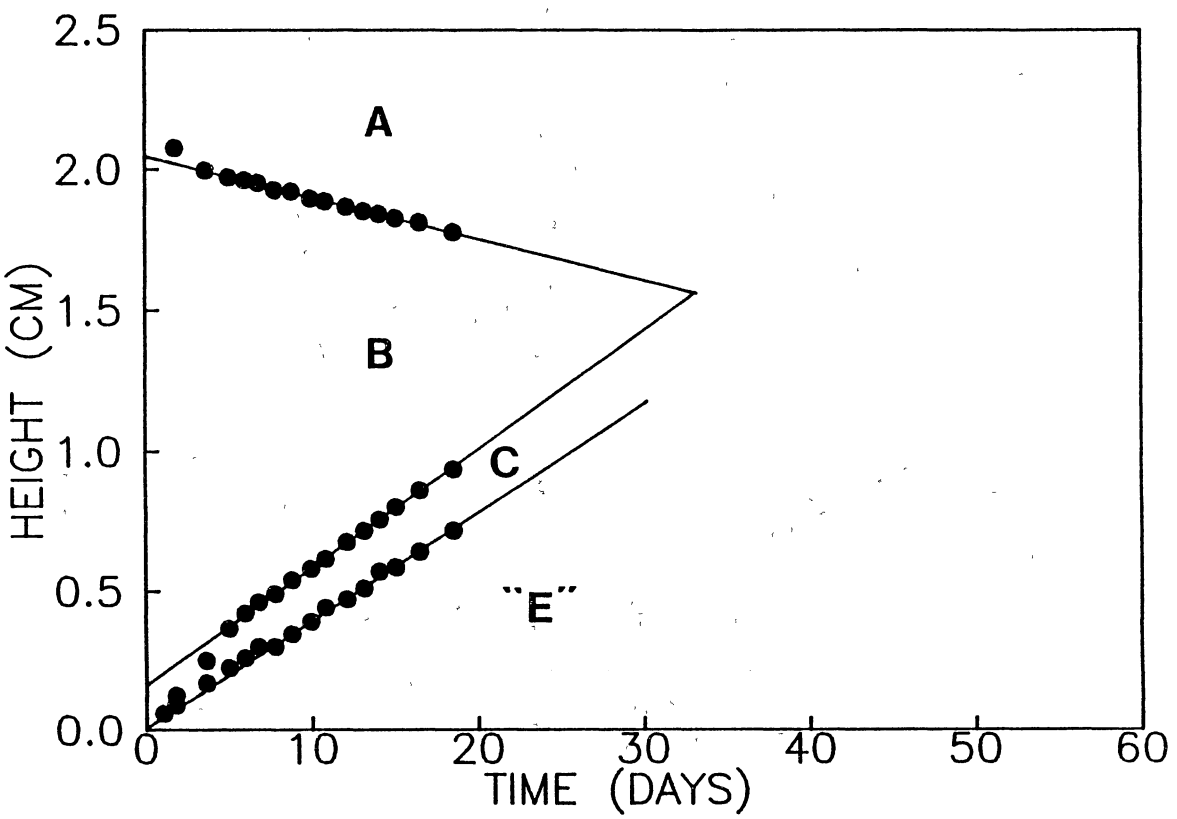

Figure 19. Sample very near the freezing transition. The columnar crystal region (E) is qualified in quotes as this region did not appear to be true columnar crystal in observation, but some transitional phase to dense polycrystalline solid. $\phi = 0.49$.

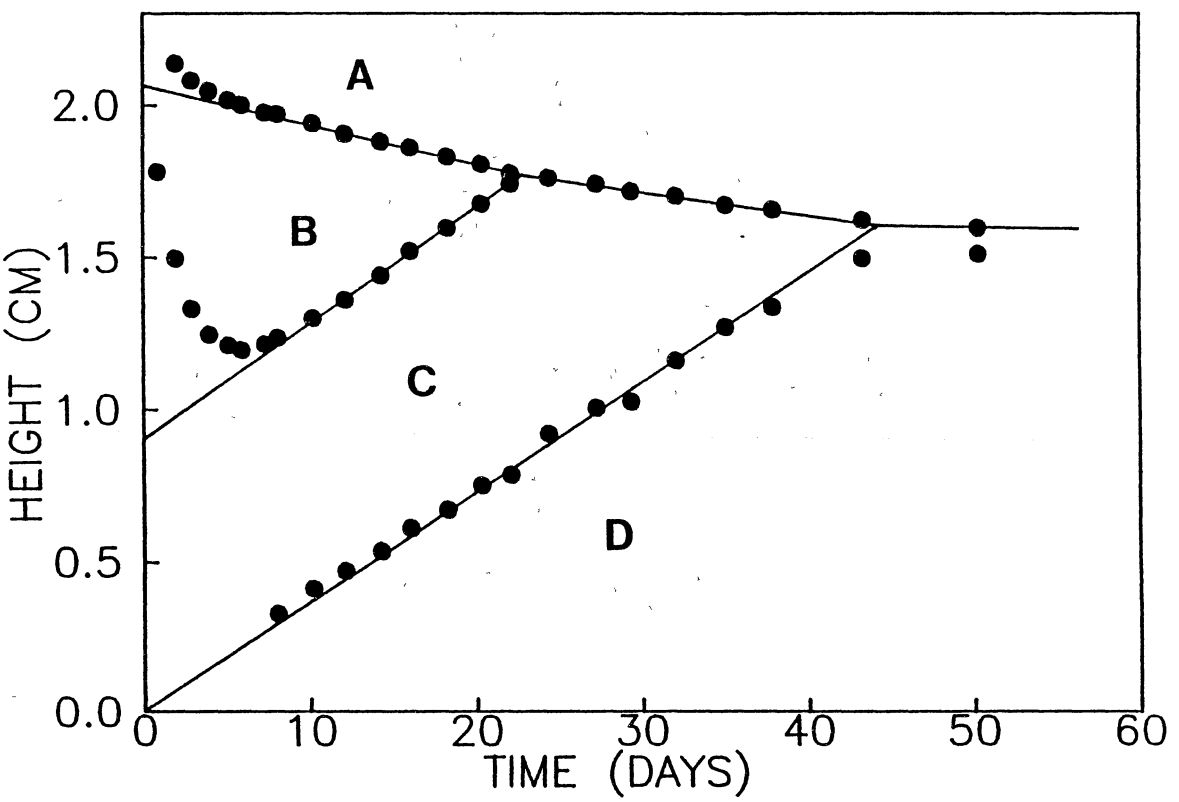

Figure 20. Sample in the coexistence region of the phase diagram. $\phi = 0.50$.

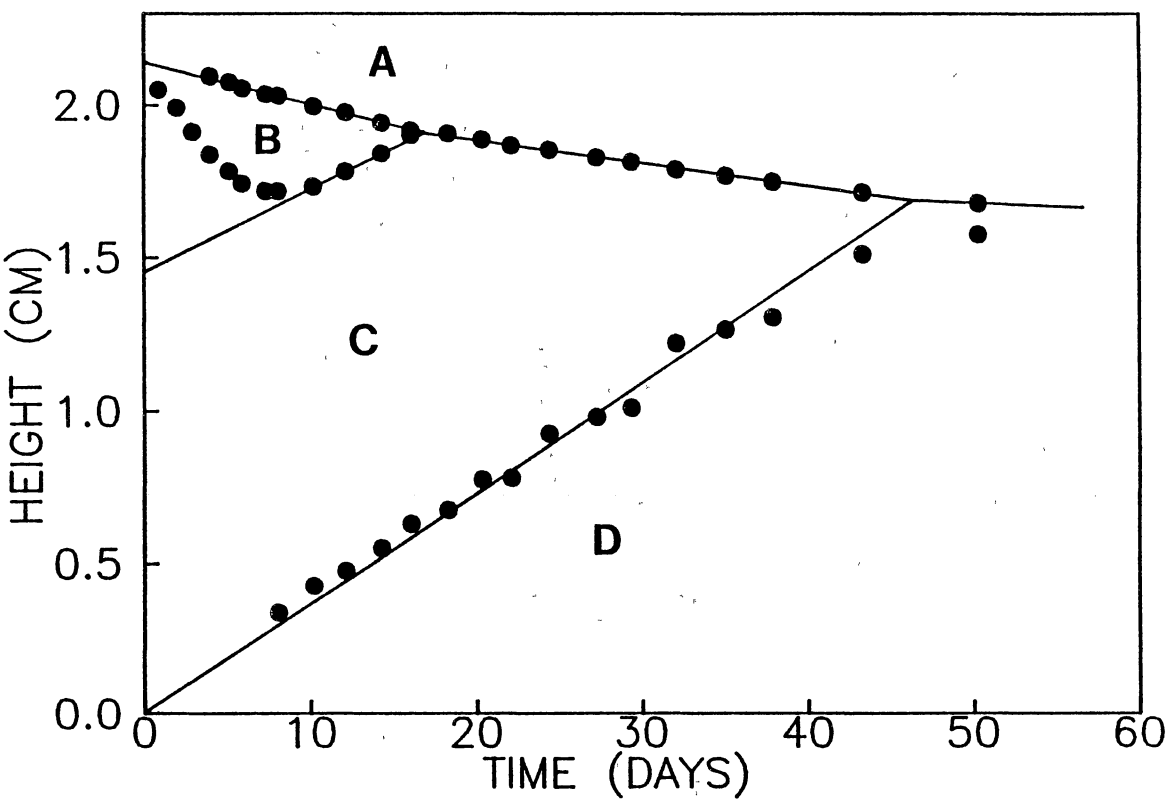

Figure 21. Sample in the coexistence region of the phase diagram. $\phi = 0.51$.

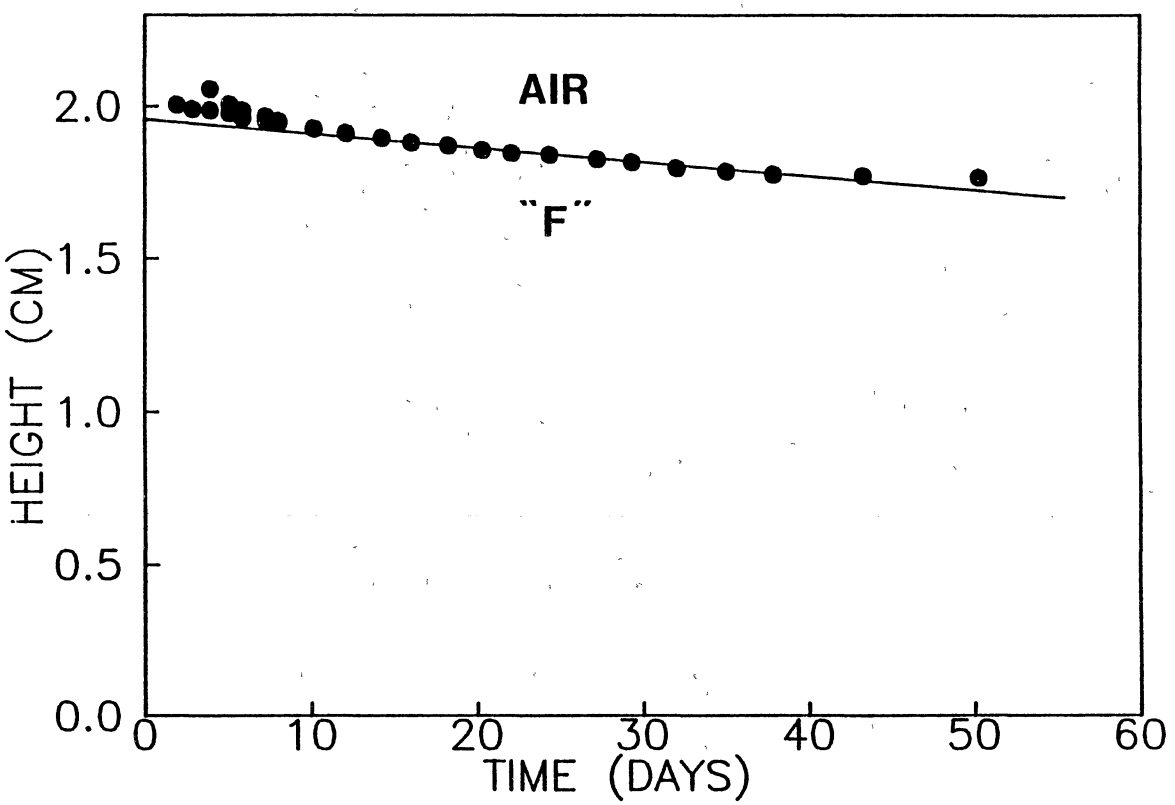

Figure 22. Sample in the glass region of the phase diagram. Here the glass region (F) is qualified in quotes as this sample appeared transitional from fully crystalline to glass. $\phi = 0.57$.

APPENDIX C

DENSITY PROFILES FOR ALL OTHER SAMPLES

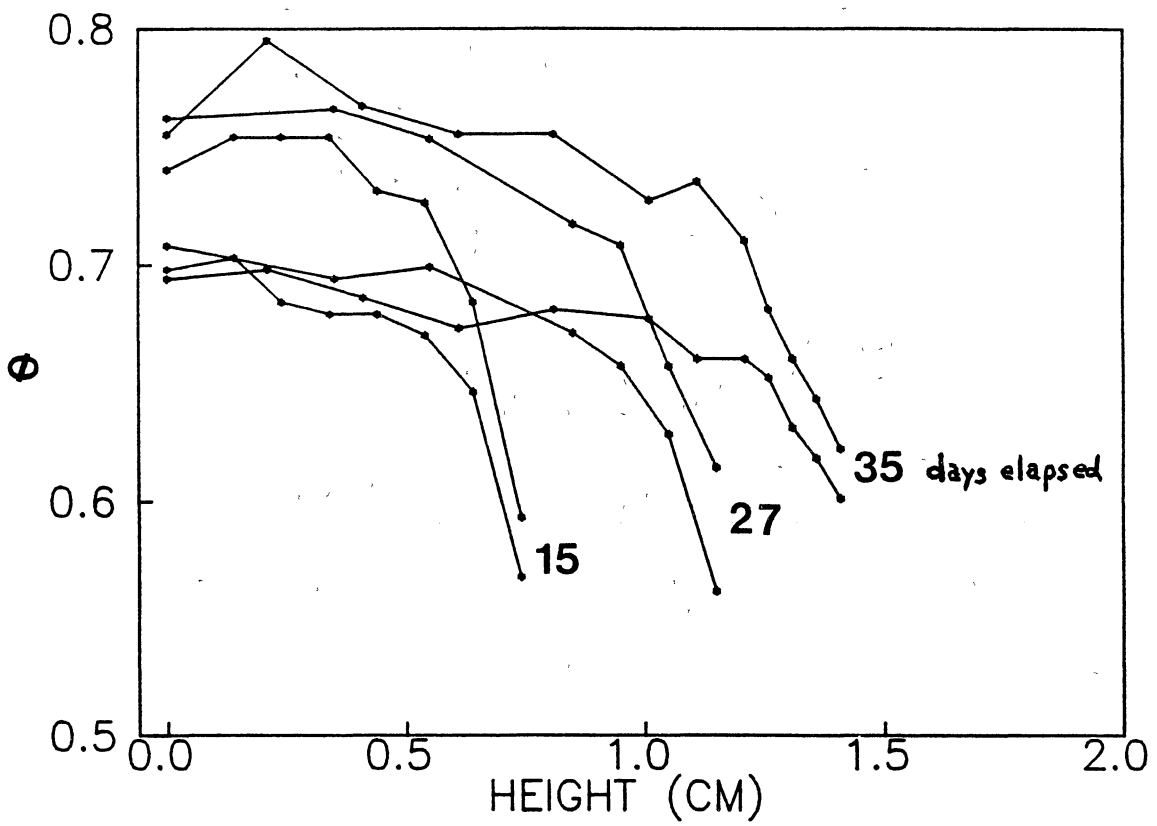

Figure 23. Sample in the liquid region of the phase diagram. $\phi = 0.42$.

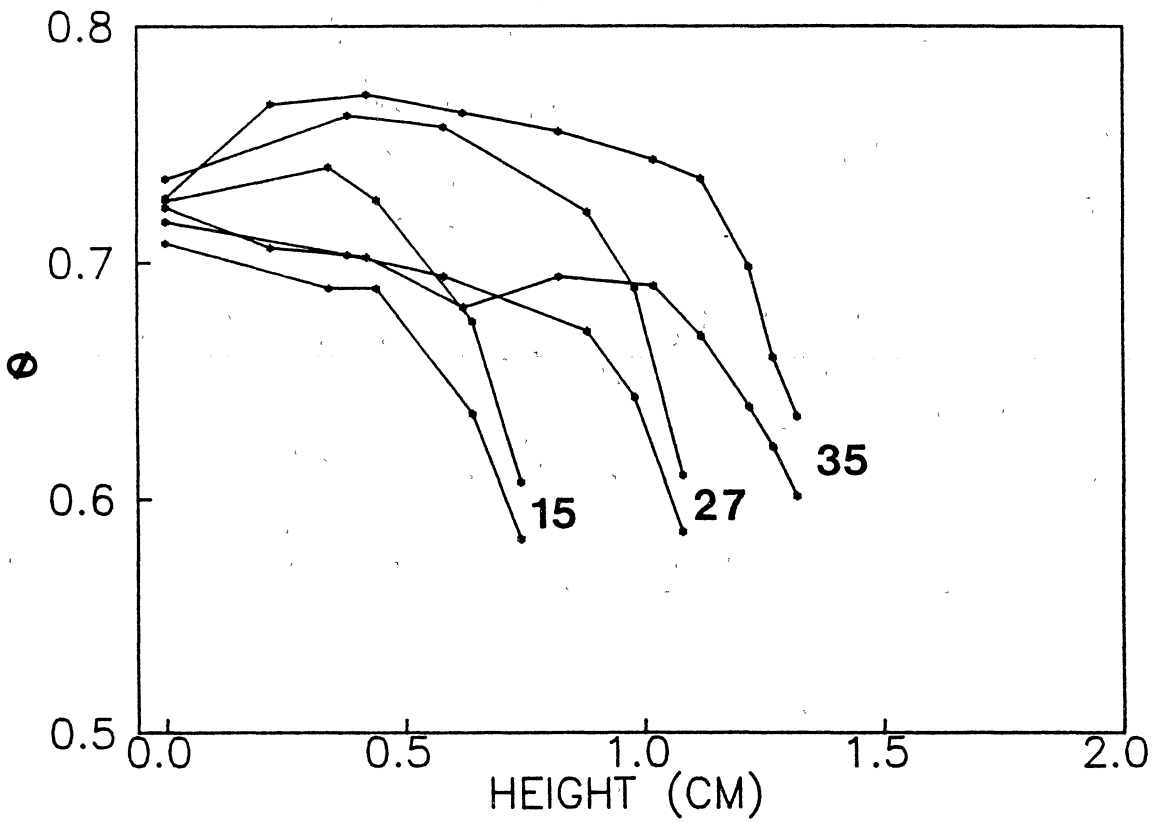

Figure 24. Sample in the liquid region of the phase diagram. $\phi = 0.46$.

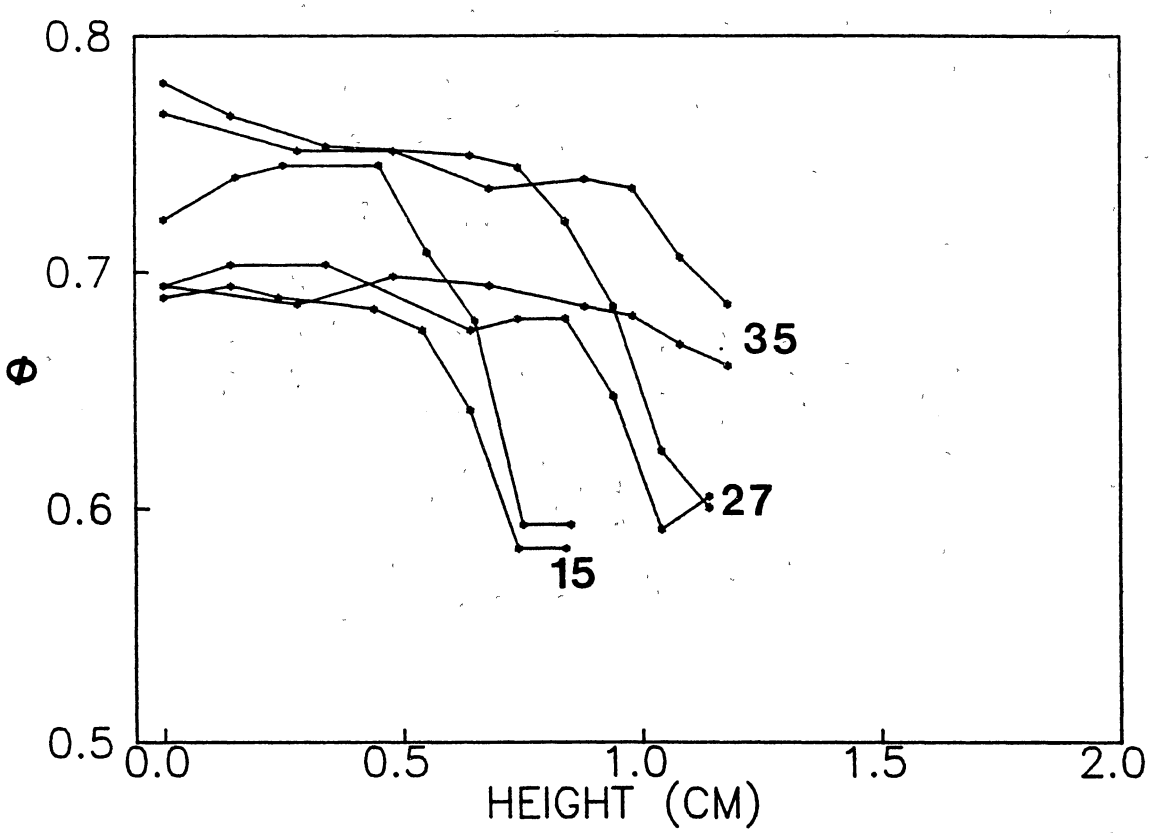

Figure 25. Sample in the coexistence region of the phase diagram. $\phi = 0.48$.

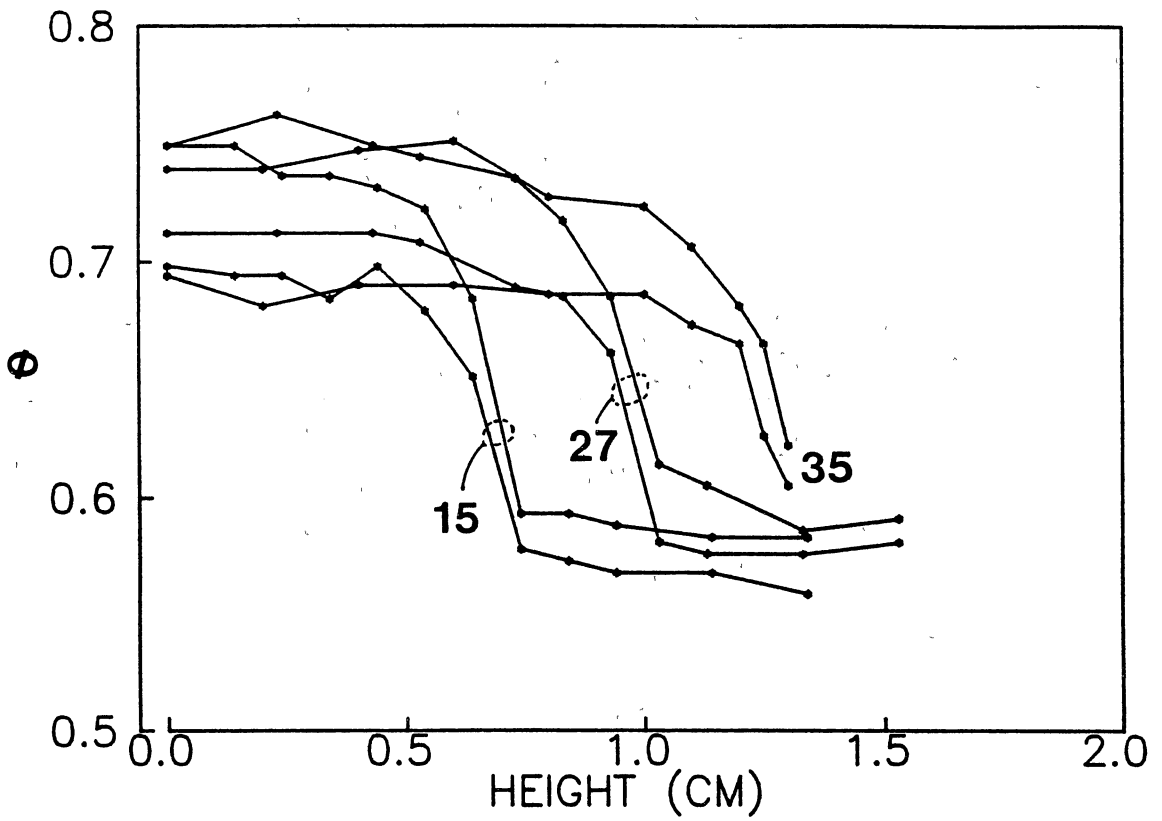

Figure 26. Sample in the coexistence region of the phase diagram. $\phi = 0.50$.

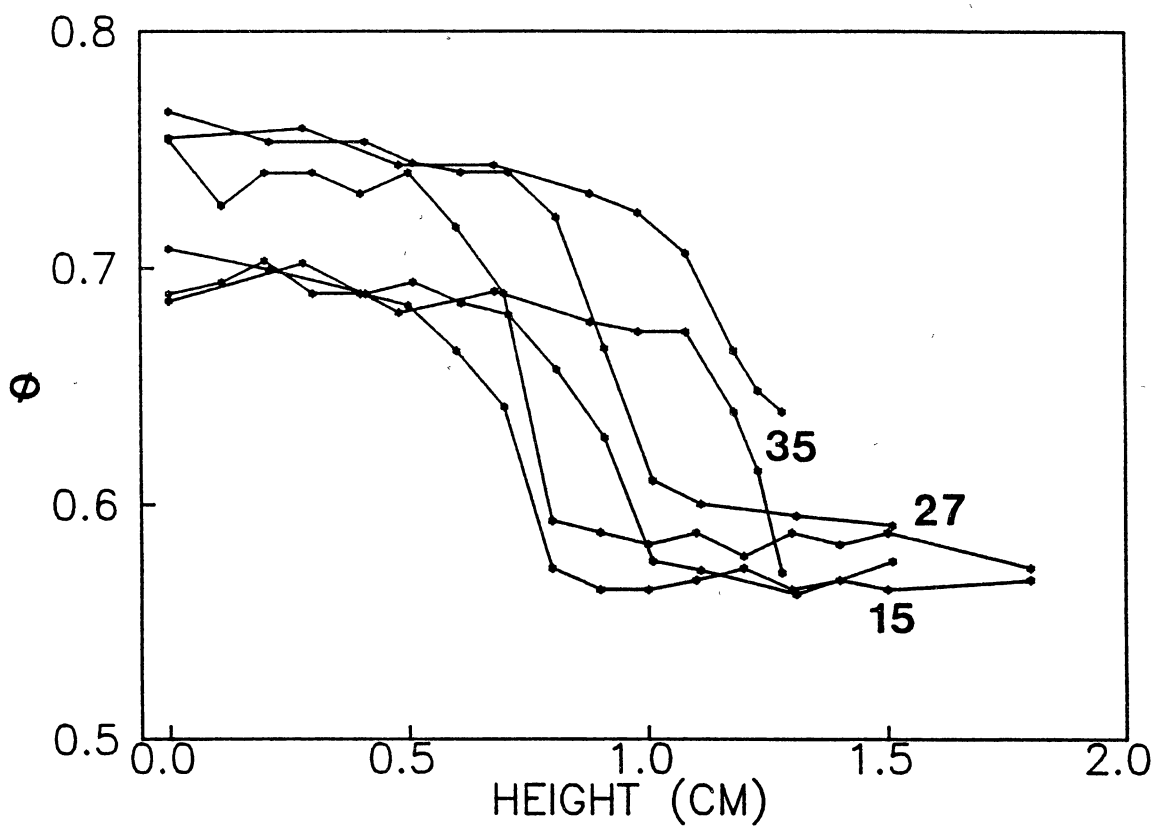

Figure 27. Sample in the coexistence region of the phase diagram. $\phi = 0.51$.

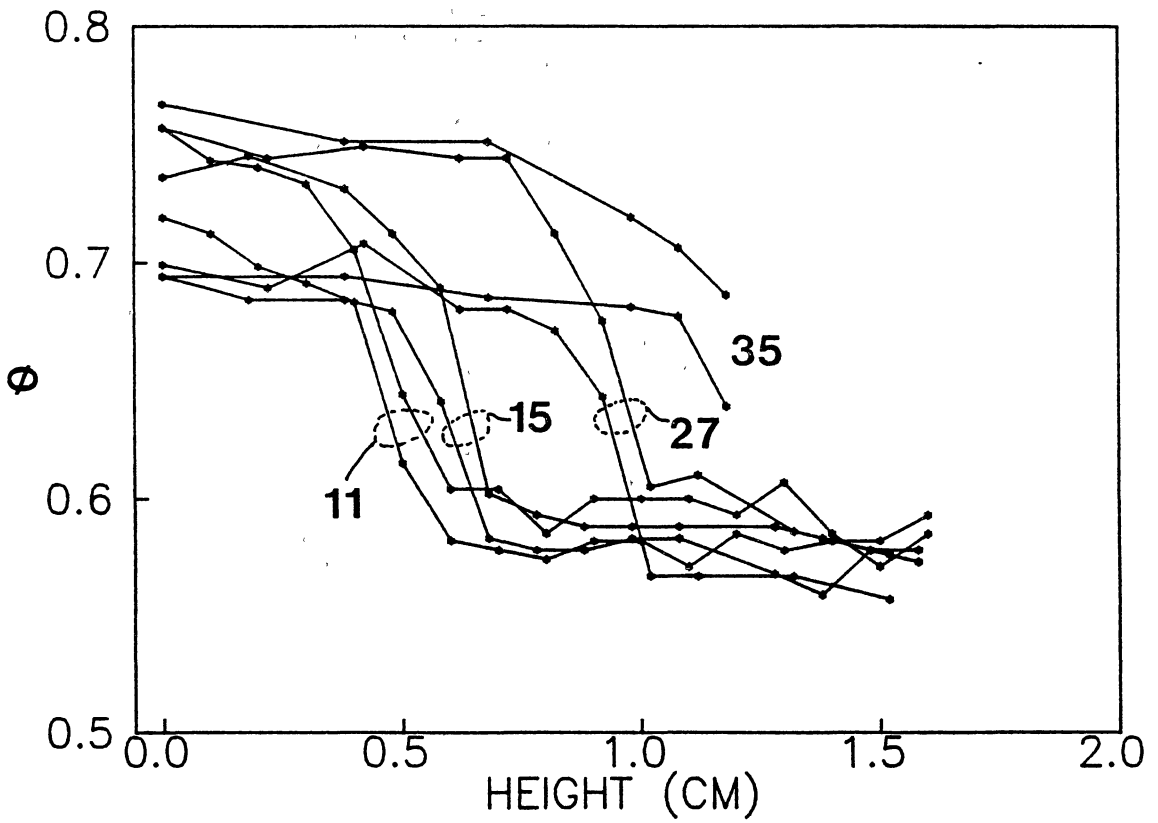

Figure 28. Sample in the fully crystalline region of the phase diagram. $\phi = 0.54$.

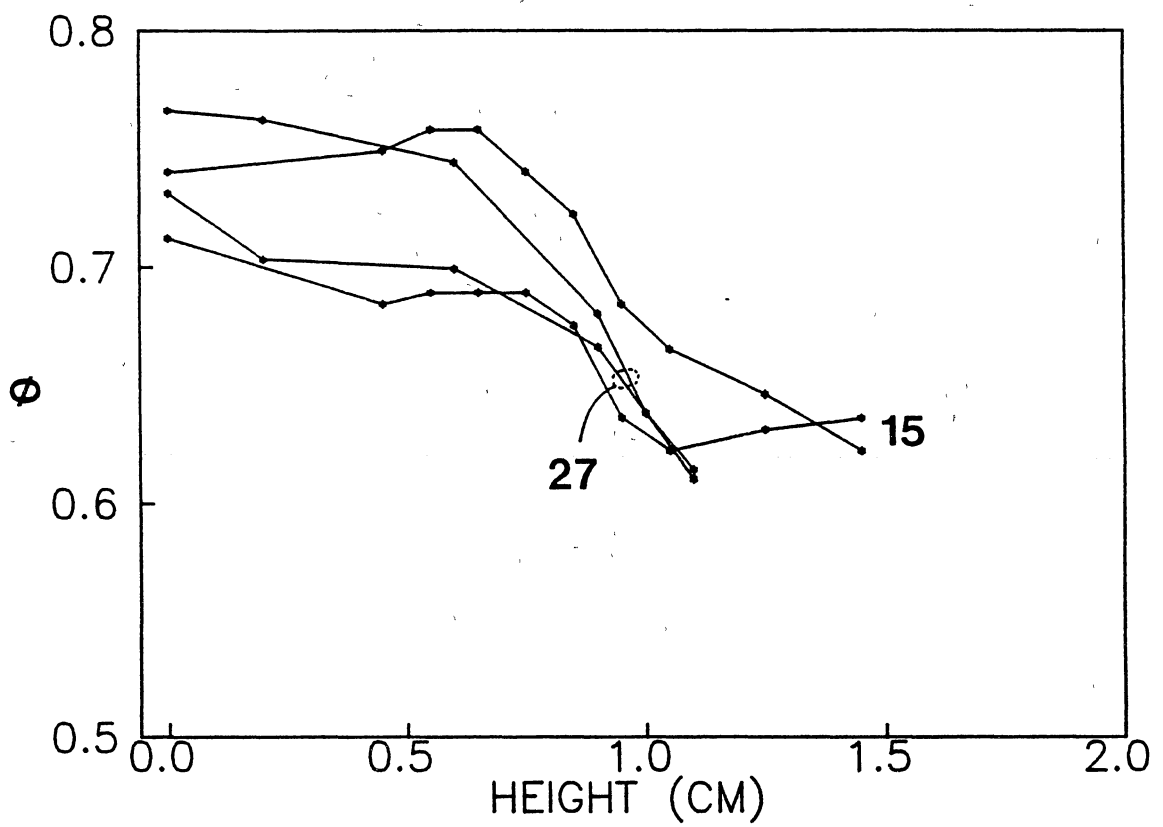

Figure 29. Sample in the glass region of the phase diagram. This sample appeared transitional from fully crystalline to glass. $\phi = 0.57$.

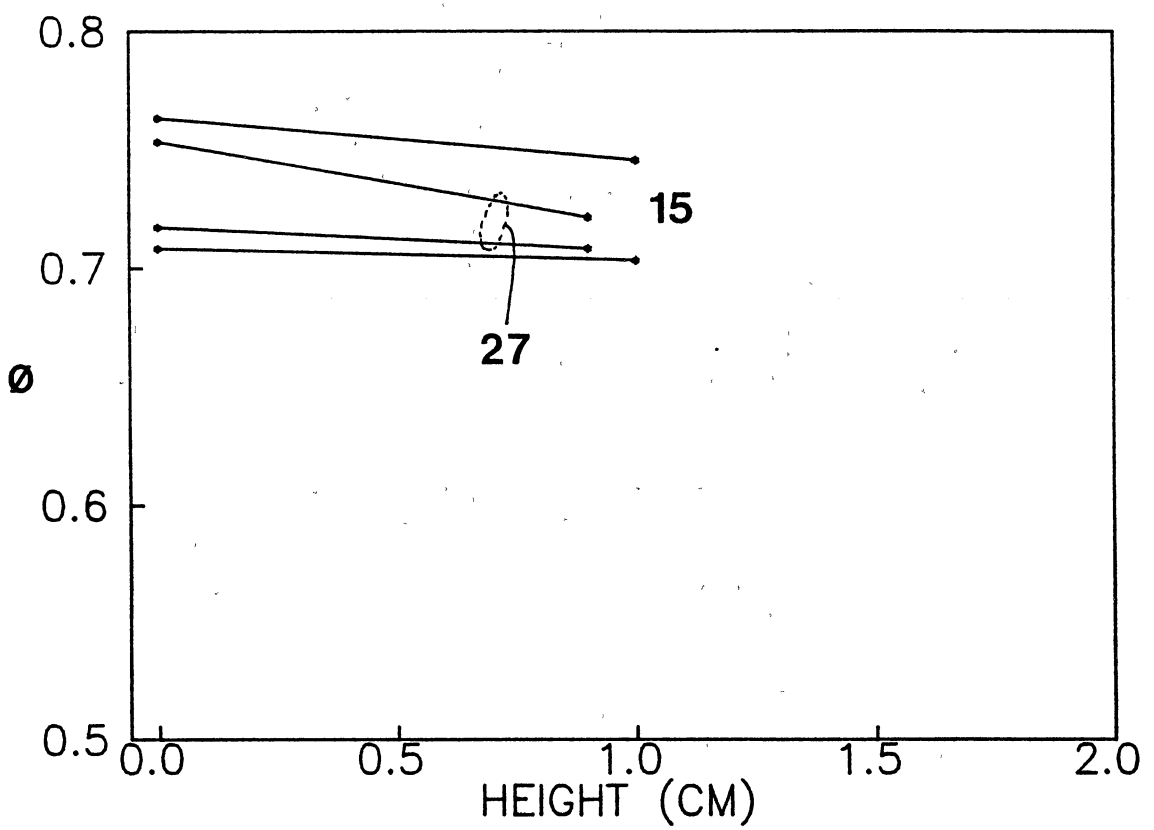

Figure 30. Sample in the glass region of the phase diagram. $\phi = 0.59$.

VITA

STEVEN EDWARD PAULIN

Candidate for the Degree of

Master of Science

Thesis: SEDIMENTATION OF PMMA SPHERES

Major Field: Physics

Biographical:

Personal Data: Born in Cleveland, Ohio, November 18, 1963, the son of Edward and Mary Jane Paulin. Married to Carol Diahann Bandy on May 5, 1990.

Education: Graduated from Padua Franciscan High School, Parma, Ohio, in May, 1982; received Bachelor of Science Degree from Cleveland State University in August 1986 with a major in physics; completed the requirements for the Master of Science Degree at Oklahoma State University in July, 1990.

Professional Experience: Undergraduate Research Assistant, Cleveland State University, January 1985 to July 1987; Graduate Teaching Assistant, Oklahoma State University, August 1987 to December 1988; Graduate Research Assistant, Oklahoma State University, January 1989 to Present.